# Global Air Pollutant Phenanthrene and Arrhythmic Outcomes in a Mouse Model

Sana Yaar,[1] Tatiana S. Filatova,[2] Ellie England,[1] Shiva N. Kompella,[1]* Jules C. Hancox,[3] David A. Bechtold,[1] Luigi Venetucci,[1] Denis V. Abramochkin,[2] and Holly A. Shiels[1]

[1]Faculty of Biology, Medicine, and Health, Division of Cardiovascular Sciences, University of Manchester, Manchester, UK
[2]Department of Human and Animal Physiology, Lomonosov Moscow State University, Moscow, Russia
[3]School of Physiology, Pharmacology and Neuroscience, University of Bristol, Bristol, UK

**BACKGROUND:** The three-ringed polycyclic aromatic hydrocarbon (PAH) phenanthrene (Phe) has been implicated in the cardiotoxicity of petroleum-based pollution in aquatic systems, where it disrupts the contractile and electrical function of the fish heart. Phe is also found adsorbed to particulate matter and in the gas phase of air pollution, but to date, no studies have investigated the impact of Phe on mammalian cardiac function.

**OBJECTIVES:** Our objectives were to determine the arrhythmogenic potential of acute Phe exposure on mammalian cardiac function and define the underlying mechanisms to provide insight into the toxicity risk to humans.

**METHODS:** *Ex vivo* Langendorff-perfused mouse hearts were used to test the arrhythmogenic potential of Phe on myocardial function, and voltage- and current-clamp recordings were used to define underlying cellular mechanisms in isolated cardiomyocytes.

**RESULTS:** Mouse hearts exposed to $\sim 8$ μM Phe for 15-min exhibited a significantly slower heart rate ($p = 0.0006$, $N = 10$ hearts), a prolonged PR interval ($p = 0.036$, $N = 8$ hearts), and a slower conduction velocity ($p = 0.0143$, $N = 7$ hearts). Whole-cell recordings from isolated cardiomyocytes revealed action potential (AP) duration prolongation (at 80% repolarization; $p = 0.0408$, $n = 9$ cells) and inhibition of key murine repolarizing currents—transient outward potassium current ($I_{to}$) and ultrarapid potassium current ($I_{Kur}$)—following Phe exposure. A significant reduction in AP upstroke velocity ($p = 0.0445$, $n = 9$ cells) and inhibition of the fast sodium current ($I_{Na}$; $p = 0.001$, $n = 8$ cells) and calcium current ($I_{Ca}$; $p = 0.0001$) were also observed, explaining the slowed conduction velocity in intact hearts. Finally, acute exposure to $\sim 8$ μM Phe significantly increased susceptibility to arrhythmias ($p = 0.0455$, $N = 9$ hearts).

**DISCUSSION:** To the best of our knowledge, this is the first evidence of direct inhibitory effects of Phe on mammalian cardiac electrical activity at both the whole-heart and cell levels. This electrical dysfunction manifested as an increase in arrhythmia susceptibility due to impairment of both conduction and repolarization. Similar effects in humans could have serious health consequences, warranting greater regulatory attention and toxicological investigation into this ubiquitous PAH pollutant generated from fossil-fuel combustion. https://doi.org/10.1289/EHP12775

## Introduction

Air pollution is one of the leading risk factors for global disease burden,[1–7] and accounts for an estimated 6.7 million premature deaths each year worldwide.[8] With 99% of the human population living with air quality that falls below World Health Organization guidelines,[9] and with air pollution levels continuing to increase in some parts of the globe, the threat of air pollution to life expectancy and life quality is ever-growing.[10] A host of epidemiological studies have shown mortality from cardiovascular disease accounts for the majority of deaths attributed to air pollution.[2,4,5,7,11–14] A 2019 European study found that of the 800,000 excess deaths per year attributed to ambient air pollution, almost half were due to ischemic heart disease and stroke.[2] There also is strong epidemiological evidence linking exposure to air pollution with cardiac arrhythmias, myocardial infarction, atherosclerosis, and heart failure.[15–17]

Air pollution is a complex mixture of gases, suspended particulate matter (PM) and liquid droplets.[18] PM with an aerodynamic diameter of $\leq 2.5$ μm ($PM_{2.5}$) is a key driver of the cardiovascular impacts of poor air quality,[19–21] in part due to the ability of small particles to translocate from the lungs into the systemic circulation.[3,19,22] Importantly, the cardiovascular toxicity of $PM_{2.5}$ reflects the surface chemistry of the particles, which consists of a diverse range of adsorbed chemicals, including reactive transition metals and polyaromatic hydrocarbons (PAHs). PAHs contain two or more fused benzene rings and are a ubiquitous component of air pollution formed during the incomplete combustion of fossil fuels.[19,23] Their cardiotoxicity became apparent following the devastating impact of two major crude oil spills (the *Deepwater Horizon* and the *Exxon Valdez*) on fish cardiovascular function.[19,24,25] Decades of research in aquatic species exposed to crude oil have revealed the three-ringed PAH phenanthrene (Phe) as the primary PAH responsible for cardiac dysfunction in fish. Phe-exposed fish showed bradycardia and atrioventricular (AV) block[26] due to inhibition of cellular calcium ($Ca^{2+}$) cycling in cardiomyocytes and altered repolarization due to inhibition of potassium ($K^+$) channels.[26–28] Further work in fish demonstrated Phe-induced cardiac dysfunction evident at the myocyte, cardiac tissue, and whole-heart levels.[27–32]

Phe also exists in polluted air in the gas phase and bound to the surface of PM.[33] Phe is present at high levels in exhaust emissions and cigarette smoke[34,35] and is consistently reported among the most abundant PAHs in the environment.[36–38] A 1994 report from London, UK, found Phe levels at 76–82 ng/m^{3} in the air.[39] Phe from the air accumulates in the body. A recent study in Greece found 2-fold higher levels of Phe compared with all other PAHs in human serum (56.5 μg/L, $\sim 300$ nM Phe).[40] Interestingly, these authors found urban vs. rural residence had a greater impact on circulating Phe levels than smoking status. Patients with heart failure in that study had mean serum levels of $\sim 1.3$ μM compared with levels ranging from 0.14 to 0.58 μM in control participants, suggesting a link between Phe serum concentration and heart failure incidence.[40] The maximum concentration of serum Phe found in patients with heart failure was 3.3 μM. Similar concentrations have been found in human urine analysis of road pavers and coke plant workers (0.2–3.5 μM).[41] Phe has also been found in mouse whole-blood samples at concentrations >5 μM following oral dosing.[42] The presence of Phe in human and murine blood analysis

**Note to readers with disabilities:** *EHP* strives to ensure that all journal content is accessible to all readers. However, some figures and Supplemental Material published in *EHP* articles may not conform to 508 standards due to the complexity of the information being presented. If you need assistance accessing journal content, please contact ehpsubmissions@niehs.nih.gov. Our staff will work with you to assess and meet your accessibility needs within 3 working days.

provides evidence that it can reach, and therefore directly interact, with the mammalian heart. Furthermore, Phe is highly lipophilic ($Kow \cong 4.4$[43]) and therefore can accumulate in tissue at higher levels than in plasma or serum, particularly in adipose tissue or adipose-rich organs, such as the liver and kidneys.[33,44,45]

Recent work has shown that acutely applied Phe directly inhibits human Ether-à-go-go-Related Gene (hERG) channels.[46] Given that hERG channels are vital for normal human ventricular repolarization, their inhibition raises the risk of Phe-associated arrhythmogenesis. The deleterious effects of Phe on fish hearts[26–32,47] also makes determining the impact of Phe on arrhythmogenic potential in a mammalian model vital. Currently, there is a paucity of research into the impact of Phe exposure in mammals. There are studies reporting cardiac hypertrophy[48] and increased inflammation[49] in rodent models of prolonged (~4 wk) Phe exposure; however, no study to date has investigated the effect of acute Phe exposure on the electrical activity of the mammalian heart. In the present study, we used the mouse to investigate the impact of acute Phe exposure on whole-heart electrical activity and arrhythmogenic potential. Our *ex vivo* heart findings are supported by characterization of the impact of Phe on the underlying ion currents in isolated mouse ventricular cardiomyocytes. We hypothesized that Phe would disrupt electrical activity in the mouse heart, resulting in increased arrhythmia susceptibility.

## Materials and Methods

### Animal Husbandry

All procedures were carried out in accordance with approval of the local animal welfare board. C57BL/6J male (Charles River Laboratories) mice were housed under a 12-h light/dark cycle, with 30%–60% relative humidity, and fed a standard mouse chow and water diet. Mice were euthanized at 10–12 wk of age by cervical dislocation. Individual mice were not weighed; the average weight of a male mouse this age is 25 g (Charles River Laboratories, https://www.criver.com/products-services/find-model/c57bl6-mouse?region=3671).

### Phe Exposures

Analytical grade Phe (>99%) was acquired from Sigma Aldrich. A 50 mM Phe stock was prepared daily by dissolving Phe in dimethyl sulfoxide (DMSO; tissue culture grade, Sigma Aldrich). The stock was then diluted into saline solution (composition below) to give an initial final concentration ranging from 1 to 30 μM Phe. The maximum initial concentration of Phe used was either 25 μM (for whole hearts) or 30 μM (for cardiomyocytes). An equivalent volume of DMSO was diluted in saline solution in control experiments. However, the exposure concentration (i.e., the concentration that arrives at the tissue) can deviate from the initial concentration owing to the hydrophobic properties of Phe. This hydrophobicity makes it difficult to maintain the desired concentration when Phe is dissolved in an aqueous solution because Phe can be lost via sorption to materials, volatilization when being gassed, and degradation due to light.[50] Although all solutions were maintained in darkened reservoirs/tubes and avoided light during experimentation, the hydrophobicity still presented challenges in the *ex vivo* heart Langendorff experiments owing to the use of the highly adsorbent silicone tubing for peristaltic perfusion and the required oxygenation. Exposure concentration was less of a concern in the myocyte experiments, where saline solutions were not gassed and were gravity delivered through polyetheretherketone high-performance liquid chromatography tubing, which is narrow, chemically resistant, and inert. To account for the loss of Phe concentration due to hydrophobicity, we calculated the exposure concentration that arrived at either the heart

in the Langendorff setup or at myocytes in the patch clamp rig by collecting perfusate at the site of tissue exposure and testing it against a standard curve using florimetry (FluoroMax-4, Horiba Scientific) at an excitation wavelength of 250 nm (slit width: 5 nm) and emission wavelength of 366 nm (slit width: 1 nm). To produce the standard curve, Phe was dissolved in ethanol (99.8% analytical grade) to make a 50 mM stock solution. The stock solution was then diluted to produce 0.5–4 μM standard concentrations with a 1:1 ratio of ethanol and physiological saline. For the Langendorff rig, the exposure concentration of our initial 25 μM dose ranged from 6.5 to 10 μM, with a mean of $8.0 \pm 0.74$ μM ($n = 6$). For the 10 μM initial dose, the exposure concentration ranged from 1 to 2.8 μM, with a mean of $2.1 \pm 0.28$ μM, ($n = 6$). Owing to the variability in exposure concentration, which is impacted by the duration and vigor of oxygenation, we opted to use the mean exposure doses of ~2.1 μM and ~8 μM for the low and high exposures in the *ex vivo* heart experiments. A similar test for variation between calculated concentration and exposure concentration in the patch clamp apparatus revealed less than a 0.2 μM variation ($n = 5$). Thus, for the myocyte work, the concentrations are provided numerically in the following sections; however, a $\pm 0.2$ μM range around each is expected.

### Assessing Ex Vivo Cardiac Electrical Activity

***Langendorff isolated heart preparation.*** Following sacrifice, the heart was rapidly excised and transferred to ice-cold physiological saline [constituents in millimoles: sodium chloride (NaCl), 118; sodium bicarbonate ($NaHCO_3$), 24; glucose, 10; monosodium phosphate ($NaH_2PO_4$), 1.2; sodium pyruvate, 2; calcium chloride ($CaCl_2$), 2; potassium chloride (KCl), 4; and magnesium sulfate ($MgSO_4$), 1.2 plus 0.06% DMSO]. The aorta was cannulated on a shortened and blunted 22-gauge cannula that was then attached to a heated glass coil. The heart was retrogradely perfused with oxygenated [carbogen gas: 95% oxygen ($O_2$)+5% carbon dioxide ($CO_2$)] physiological saline maintained at 37°C, at a constant rate of 4 mL/min. Spontaneously beating hearts were allowed to stabilize for at least 10-min until a stable heart rate (HR) was achieved. Following a 15-min baseline recording period, perfusion was switched so that exposure was either ~2.1 μM or ~8 μM Phe for 15-min. Finally, perfusion was switched back to control saline solution for a 15-min wash-out period. In time-matched control experiments, hearts were exposed to saline solution plus DMSO vehicle control only.

***Cardiac electrical parameter recordings.*** Electrocardiographs (ECGs) were recorded using specialized surface electrodes, placed just below the right atrium and on the apex of the heart ($N = 5$–10 hearts per group). ECG recordings were analyzed using the LabChart Pro 8 software (AD instruments) with all ECG parameters—including HR and RR, QT, and PR intervals—calculated using the cardiac axis tool. A representative ECG showing measured parameters is provided in Figure S1A. The QT interval was automatically corrected in LabChart using the Mitchell formula: $QT_C = QT/\sqrt{RR}/100$.[51] Mean values for ECG parameters were calculated from 100 beats. Owing to variability in ECG recordings, it was not possible to calculate all ECG parameters for each experiment; therefore, the $N$-values for each parameter may vary.

Ventricular monophasic action potentials (MAPs) were recorded using homemade electrodes placed on the epicardial surface of the left ventricle. The peak analysis tool in LabChart was used to calculate AP durations (APDs) at 80% repolarization to give $APD_{80}$. Average $APD_{80}$ values were calculated from six consecutive beats. Monophasic $APD_{80}$ ($MAPD_{80}$) values were manually corrected for the peak–peak interval (PP) using an adapted version of the Mitchell formula: $cMAPD = MAPD80/\sqrt{PP}/100$.[51]

Cardiac electrical maps were recorded from the surface of the left ventricle ($N = 5–7$ hearts per group) using a 64-channel multi-electrode array pen (Mapping Lab). EMap Scope software was used to extract the activation time at each channel; the change in activation time across the 64-channels was used to calculate conduction velocity (in millimeters per millisecond) across the ventricle.

### Assessing Arrhythmia Susceptibility

Hearts were isolated, perfused, and allowed to stabilize as described above. ECG electrodes were placed as previously described and ECG recordings were used to assess arrhythmia susceptibility ($N = 9$ hearts per group). Hearts were exposed to $\sim 8$ µM Phe or control saline solution; after 15-min, all hearts were subjected to a programmed electrical stimulation (PES) protocol. Ventricular arrhythmias were induced using an established protocol[52,53]; briefly, an S1 train consisting of 20 pulses at a 98-ms cycle length was immediately followed by an S2–S10 train of extra stimuli. Extra-stimuli cycle lengths ranged from 58 ms down to 8 ms, decreasing in 10-ms intervals. Each segment of stimulation was separated by a 3-s gap, with a total of six segments. Ventricular tachycardia (VT) was characterized according to the Lambeth convention[52] and was defined as a train of at least four consecutive ventricular premature beats following the stimulation period. Arrhythmia susceptibility was scored according to Clasen et al.[54] (Table 1). Scores were given for each stimulation segment and average values from all six segments were calculated to give a final score for arrhythmia susceptibility. The effective refractory period (ERP) was measured from the ECG recordings as the duration of the last interval before the heart stops responding during the PES protocol.

### Assessing Cardiomyocyte Electrical Activity

**Cardiomyocyte isolation.** Ionic currents were recorded in freshly isolated ventricular cardiomyocytes from C57BL/6J male mice (Charles River Laboratories) held at Lomonosov Moscow State University, Russia, under the same husbandry conditions as cited above and in adherence to local animal ethics regulations. Each mouse was euthanized as described above, and the heart was excised and mounted onto a constant flow Langendorff apparatus for retrograde perfusion through the aorta. The heart was first perfused with nominally $Ca^{2+}$-free solution [constituents in millimoles: NaCl, 125; KCl, 4; $NaH_2PO_4$, 1.7; $NaHCO_3$, 25.2; magnesium chloride ($MgCl_2$), 1.1; sodium pyruvate, 5; glucose, 11; taurine, 30; and 4-(2-hydroxyethyl)-1-piperazineethanesulfonic acid (HEPES), 10 and 1 g/mL bovine serum albumin]; pH 7.4 buffered with carbogen gas (95% $O_2$+5% $CO_2$) at 37°C; the flow rate was set at 2 mL/min. Five minutes after the heart stopped beating, the perfusion was switched to enzymatic solution of the same composition provided with 0.5 mg/mL of collagenase II (Worthington) and 8 µM $CaCl_2$. After 30–35 min of enzymatic treatment, the perfusion was stopped, the ventricles were minced and gently triturated to release cells into the Kraftbrühe solution[55] of the following composition (in millimoles): $MgSO_4$, 3; KCl, 30; monopotassium phosphate ($KH_2PO_4$),

30; egtazic acid [Ethylene glycol-bis(2-aminoethylether)-N,N,N′,N′-tetraacetic acid (EGTA)], 0.5; potassium glutamate, 50; HEPES, 20; taurine, 20; and glucose, 10; pH 7.2 at room temperature (RT, 24°C). The cells were stored in Kraftbrühe solution at RT and used within 8 h of isolation.

**Whole-cell patch clamp.** Ionic currents and APs were recorded using conventional whole-cell patch clamp (Axon Instruments Axopatch 200a, Molecular Devices; and EPC 800USB, Heka). A small aliquot of cells was placed into an experimental chamber (RC-26, Warner Instruments Corp.) and mounted onto an inverted microscope (Diaphot 200, Nikon). The cells were superfused with physiological saline at RT ($\sim 24$°C) (composition detailed below). Thus, the cellular experiments were conducted at a lower temperature than the whole-heart experiments. The lower temperature may improve the ability to resolve impacts of exposure and also allow for comparison with other studies conducted at RT.[28] Moreover, the impact of temperature on mouse myocyte ionic currents is well established and was considered in interpreting our data. However, the authors acknowledge that future work should test the cellular findings at the body temperature of the mouse.

Patch pipettes were pulled (Narishige PC010) from borosilicate glass capillaries and filled with pipette solution (details given for each current below). The resistance of the pipette tip was 2–3 MΩ. After establishing the whole-cell configuration, series resistance and cell capacitance were compensated. Current amplitude was normalized to cell capacitance (pA/pF) during analysis. The charge carried by the whole-cell currents was calculated as the time integral of the inactivating part of the current and normalized by cell capacitance (pC/pF). The time constants of current inactivation were assessed by fitting the inactivating part of the current with first- ($I_{Kur}$, $I_{to}$, and $I_{Ca}$) or second-order ($I_{Na}$) exponential functions using Chebyshev transformation tool in Clampfit software (version 10.3, Molecular Devices) as $I = Ae^{(-t/\tau)}+C$, where $I$ represents the current amplitude at time $t$; $A$ represents the amplitude of deactivating current components, fitted with time constants tau ($\tau$); and $C$ represents any residual unfitted current.

For APs ($n = 8$ cells from $N = 4$ hearts per group) and $K^+$-current recordings ($n = 7–8$ cells from $N = 5–6$ hearts per group), the external saline contained (in millimoles) NaCl, 150; KCl, 5.4; $MgCl_2$, 1.2; $CaCl_2$, 1.8; HEPES, 5; glucose, 10; pH 7.4 adjusted with sodium hydroxide (NaOH) at RT. The pipette solution contained (in millimoles) KCl, 140; $MgCl_2$, 1; EGTA, 5; HEPES, 10; MgATP, 4; disodium guanosine 5′-triphosphate sodium salt hydrate ($Na_2GTP$), 0.03; pH 7.2 adjusted with potassium hydroxide (KOH) at RT. For recording $I_{Kur}$, the membrane was depolarized from $-80$ mV to $-40$ mV for 200 ms and then to $+40$ mV for 700 ms. For recording $I_{to}$, the membrane was depolarized from $-80$ mV to 40 mV for 500 ms. At the end of each experiment, the cell was exposed to a current blocker: 100 µM 4-aminopyridine for $I_{Kur}$ recordings; 3 mM 4-aminopyridine for $I_{to}$ recordings. The peak currents were calculated after the subtraction of the current recorded in the presence of the specific blocker. APs were evoked by injection of supra-threshold depolarizing current at 0.5 Hz in current-clamp mode.

For L-type $Ca^{2+}$ ($I_{Ca}$)-channel recordings ($N = 6–10$ cells from $N = 5$ hearts per group), the external saline contained (in millimoles) NaCl, 150; cesium chloride (CsCl), 5.4; $MgCl_2$, 1.2; $CaCl_2$, 1.8; HEPES, 5; glucose, 10; pH 7.4 adjusted with NaOH at RT. The external saline was additionally supplied with 10 µM nifedipine to inhibit L-type $Ca^2$-channels. The pipette solution contained (in millimoles): CsCl, 130; $MgCl_2$, 1; EGTA, 5; HEPES, 10; triethanolamine (TEA-Cl), 10; MgATP, 4; $Na_2GTP$, 0.03; pH 7.2 adjusted with KOH at RT. For recording $I_{Ca}$, the membrane potential was depolarized from $-80$ mV to $-40$ mV for 100 ms and then to 0 mV for 300 ms. The peak current was calculated after the subtraction of the residual current recorded in the

**Table 1.** Arrhythmia susceptibility characterization.

| Arrhythmic event | Score |
| --- | --- |
| Premature ventricular complex | 1 |
| Couplet | 3 |
| Triplet | 4 |
| Ventricular tachycardia | |
| <1 s | 5 |
| >1 s | 6 |

Note: Scoring according to Clasen et al.[54]; the higher the score, the greater the susceptibity to arrhythmia.

**Table 2.** Peak amplitude (pA·pF$^{-1}$) of $I_{Kur}$, $I_{to}$, $I_{Ca}$, and $I_{Na}$ under control conditions and after acute exposure to phenanthrene (Phe) in isolated ventricular murine myocytes.

| | Control | Phe (0.3 μM) | Phe (1 μM) | Phe (3 μM) | Phe (10 μM) | Phe (30 μM) |
|---|---|---|---|---|---|---|
| $I_{Kur}$ | $17.05 \pm 1.23$ | — | $14.32 \pm 1.58^*$ | $13.42 \pm 2.27^{**}$ | $12.41 \pm 2.01^{***}$ | $9.90 \pm 1.47^{**}$ |
| $I_{to}$ | $25.74 \pm 2.05$ | — | $20.50 \pm 3.65^*$ | $20.79 \pm 3.9^{***}$ | $17.77 \pm 3.02^{***}$ | $17.41 \pm 2.2^{**}$ |
| $I_{Ca}$ | $-4.8 \pm 0.29$ | $-5.07 \pm 0.67$ | $-4.14 \pm 0.56$ | $-3.88 \pm 0.51^{**}$ | $-3.08 \pm 0.4^{***}$ | $-2.76 \pm 0.3^{***}$ |
| $I_{Na}$ | $-49.39 \pm 2.02$ | — | $-47.83 \pm 2.94^*$ | $-39.56 \pm 3^{**}$ | $-43.37 \pm 2.9^{***}$ | $-33.53 \pm 4.19^{**}$ |

Note: Data are means ± SEMs. $I_{Kur}$, $n = 7$–8 cells from $N = 6$ hearts; $I_{to}$, $n = 7$–8 cells from $N = 5$ hearts; $I_{Ca}$, $n = 6$–10 cells from $N = 5$ hearts; $I_{Na}$, $n = 6$–7 cells from $N = 4$ hearts. —, Not applicable; ANOVA, analysis of variance; $I_{Ca}$, calcium current; $I_{Kur}$, ultrarapid potassium current; $I_{Na}$, fast sodium current; $I_{to}$, transient outward potassium current; pA·pF$^{-1}$, current amplitude normalized to cell capacitance; SEM, standard error of the mean. Significant from control, repeated measures ANOVA, $^*p < 0.05$, $^{**}p < 0.01$, and $^{***}p < 0.001$.

presence of the selective $I_{Ca}$ blocker, nifedipine (10 μM). The fast Na$^+$-current ($n = 6 - 7$ cells from $N = 4$ hearts per group) was recorded with an external solution containing (in millimoles) Tris-Cl, 120; NaCl, 20; CsCl, 5.4; MgCl$_2$, 1.2; CaCl$_2$, 1.8; HEPES, 5; glucose, 10; pH 7.4 adjusted with NaOH at RT, whereas the pipette solution contained (in millimoles) CsCl, 130; NaCl, 10; MgCl$_2$, 1; EGTA, 5; HEPES, 10; MgATP, 4; Na$_2$GTP, 0.03; pH 7.2 adjusted with KOH at RT. For recording $I_{Na}$, the membrane potential was depolarized from $-120$ mV to $-30$ mV for 40 ms. Waveform protocols can also be found in the figure legends.
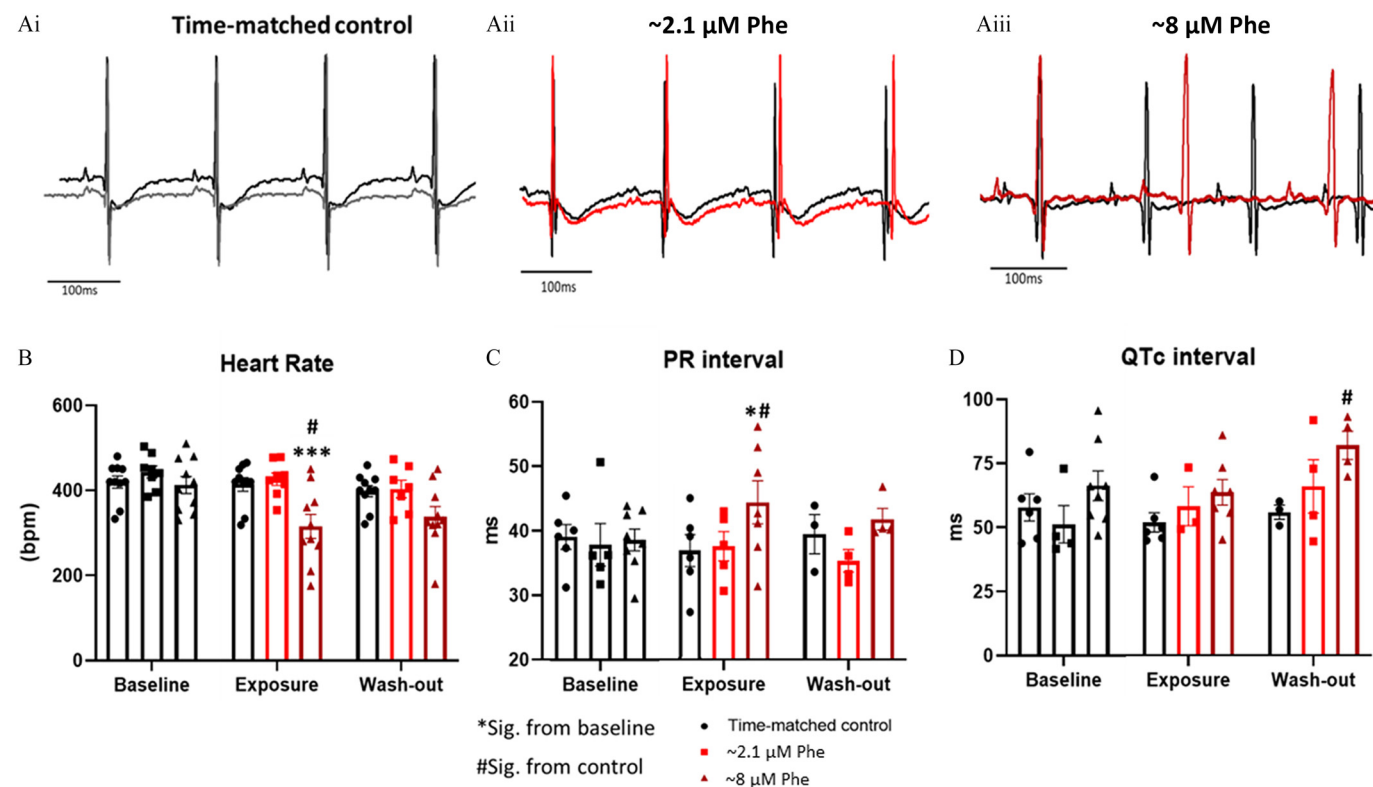
### Simplified Computational Model

To improve extrapolation from mouse to human, we used estimations of the 50% inhibitory concentration (IC$_{50}$), Hill coefficient n(H), and maximal block (Table S1) based on fractional block calculations for $I_{to}$, $I_{Ca}$, and $I_{Na}$ densities (Table 2) and set 0 concentration to 0 block and maximal possible inhibition by any

concentration to 100%. The delayed rectifying potassium channel current ($I_{Kr}$) was used in the place of $I_{Kur}$ to evaluate the impact of Phe on the human action potential, employing prior published potency against hERG1a/1b[46] using an online modeling tool.[56] The O'Hara Rudy CiPA 2017 model was selected within the ActionPotential-Portal, and APs were elicited at a stimulation rate of 1 Hz.[56,104]

### Statistical Analysis

For the cellular studies, a range of Phe concentrations (1, 3, 10, and 30 μM) was examined for each ionic current and each cell was tested under control conditions and at two concentrations applied in an ascending manner. The exact combination of doses was randomized, and thus inhibition across all doses was assessed using a two-way analysis of variance (ANOVA) mixed-effects analysis followed by Sidaks multiple comparisons test, which accounted for differing degrees of repeated measures within the



**Figure 1.** Effect of phenanthrene (Phe) exposure on *ex vivo* cardiac electrical activity in isolated murine hearts. Electrocardiograms (ECGs) were recorded from isolated hearts using surface electrodes. (A) Representative ECG traces from isolated mouse (C57/BJ, male, 10–12 wk old) hearts at baseline (black) and after 15-min exposure to either control solution (Ai, gray), $\sim 2.1$ μM Phe (Aii, red) or $\sim 8$ μM Phe (Aiii, dark red). (B) Heart rate, (C) PR interval, and (D) QTc interval from isolated hearts at baseline, after a 15-min exposure period, and finally following a 15-min wash-out period. Significantly different from baseline, $^{***}p < 0.001$, two-way ANOVA mixed-effects analysis, $N = 7$–10 hearts, $^*p < 0.05$, $N = 5$–7 hearts. Significantly different from time-matched control, mixed-effects analysis, $^\#p < 0.05$, $N = 7$–10 hearts/group. Bars are means ± SEMs, symbols are data from individual hearts. A representative mouse ECG showing the waveform and measured parameters is provided in Figure S1A and numeric values are provided in Excel Table S1. Note: ANOVA, analysis of variance; SEM, standard error of the mean; Sig, significant.

data sets. Data are provided as percentage inhibition in the figures and as absolute changes in peak current in Table 2. The percentage data were analyzed using ANOVA on ranks/Kruskal-Wallis with Dunn's multiple comparisons test. Categorial data were analyzed using a chi-square test. Analysis and graphing were performed in GraphPad Prism (version 8). The specifics for each statistical test are also described in the figure legends and results along with $p$-values, $N$ numbers for hearts, and $n$ numbers for myocytes.

## Results

### Impact of Phe on Cardiac Electrical Activity in Murine Hearts and Cardiomyocytes

Acute exposure to $\sim 8\ \mu$M Phe caused a significant prolongation of the RR interval (Figure 1A). Figure 1B shows the mean HR (calculated as the number of beats per minute) at baseline and after exposure to either control solution, $\sim 2.1\ \mu$M Phe or $\sim 8\ \mu$M Phe. A significant reduction in HR was observed in $\sim 8\ \mu$M Phe-treated hearts only (average reduction of $87 \pm 20$ bpm; two-way ANOVA mixed-effects analysis, $p = 0.0006$, $N = 10$ hearts). A 15-min wash-out period did not restore the HR to baseline levels. In contrast, no significant changes in HR were observed at $\sim 2.1\ \mu$M Phe (mean HR; baseline 431 bpm, $\sim 2.1\ \mu$M Phe exposure 416 bpm). A significant prolongation of the PR interval was also observed at $\sim 8\ \mu$M Phe (Figure 1C; two-way ANOVA mixed-effects analysis, $p = 0.036$, $N = 8$ hearts), again with no

wash-out. Corrected QT interval (QTc; corrected for HR using the Mitchell formula) showed no significant effects of Phe at any dose (Figure 1D). No changes were observed in other ECG parameters (uncorrected QT, QRS-duration, or P-wave duration) following acute Phe exposure (Figure S1).

Ventricular MAPs recorded from the epicardial surface of $\sim 8\ \mu$M Phe-exposed hearts ($N = 6$) showed a prolongation compared with time-matched controls (Figure 2A). However, when corrected for HR (PP interval, cMAPD$_{80}$; Figure 2B) the effect was lost. Similarly, MAPD$_{50}$ was not altered following Phe exposure (Figure S2). Phe effects on APD were also evaluated in isolated cardiomyocytes using whole-cell current-clamp to record APs prior to and during application of 30 $\mu$M Phe. Figure 2C shows a representative trace. Hearts exposed to Phe exhibited a 22.5% prolongation of the ventricular AP at 50% (Figure 2Di; APD$_{50}$, paired $t$-test, $p = 0.0499$, $n = 9$ cells from $N = 4$ hearts) and a 32% prolongation at 80% repolarization (Figure 2Dii; APD$_{80}$, paired $t$-test, $p = 0.0408$, $n = 9$ cells from $N = 4$ hearts) compared with control hearts. An 8% reduction in both upstroke velocity (Figure 2Diii; dV/dt, paired $t$-test, $p = 0.0445$, $n = 9$ cells from $N = 4$ hearts) and AP amplitude (Figure 2Div; $5 \pm 1.3$ mV reduction, paired $t$-test, $p = 0.005$, $n = 9$ cells from $N = 4$ hearts) was also observed in cardiomyocytes following 30 $\mu$M Phe exposure. However, lower doses ($\leq 10\ \mu$M) did not affect APD parameters, and exposure at any dose did not affect the resting membrane potential (RMP; Figure 2C and Excel Table S2).
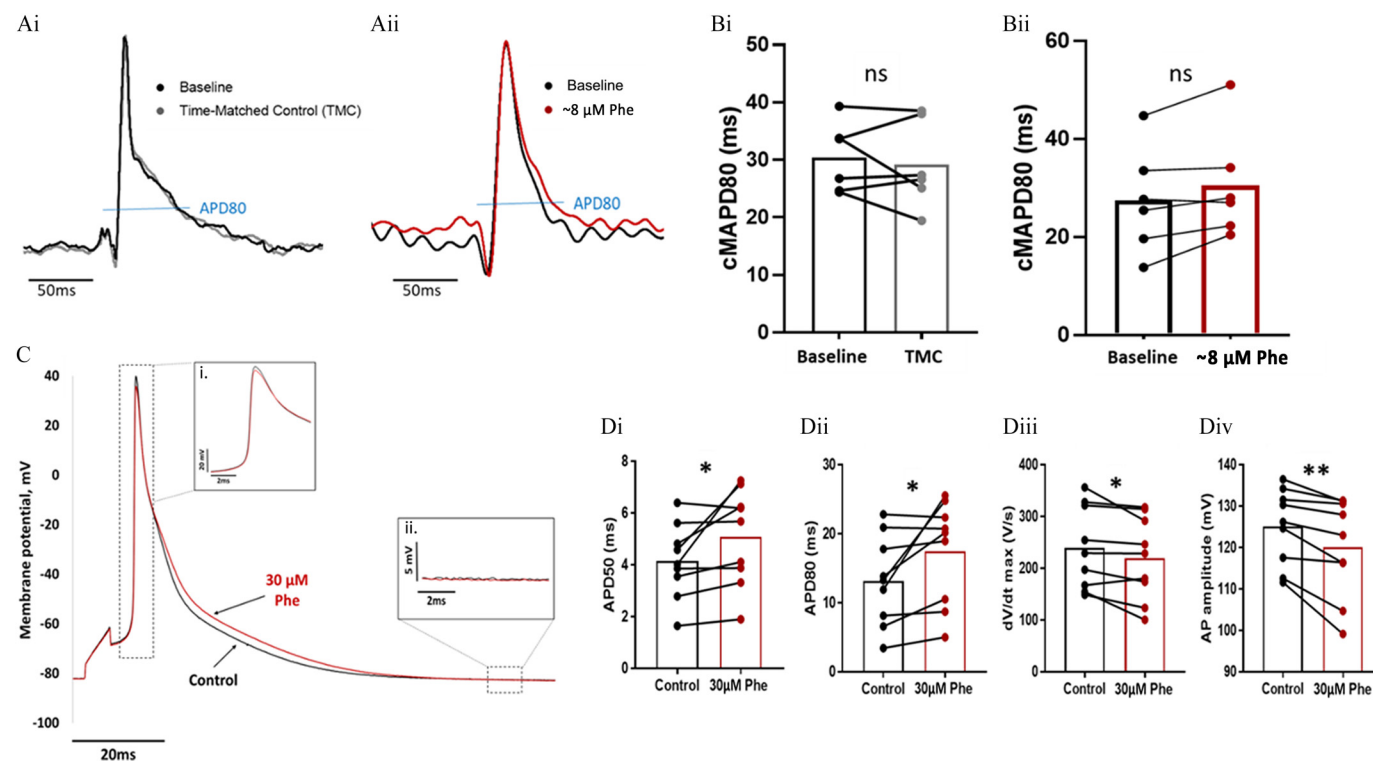


**Figure 2.** Effect of phenanthrene (Phe) on ventricular repolarization. (A) Impact of Phe on ventricular monophasic action potentials (MAPs) recorded from the surface of isolated hearts in control (Ai) and Phe-exposed (Aii) conditions at baseline (black) and after a 15-min exposure period to $\sim 8\ \mu$M (dark red) or time-matched controls (gray). Scale bar: 50 ms. Blue line indicates 80% repolarization. (B) MAP duration at 80% repolarization, corrected for peak–peak interval (cMAPD$_{80}$) at baseline and after exposure to either time-matched control solution (Bi) or $\sim 8\ \mu$M Phe (Bii). $N = 6$ hearts, each point represents an individual heart, with lines showing impact from exposure. (C) Impact of Phe on cellular action potentials (APs) measured from isolated murine ventricular myocytes using whole-cell current-clamp. Original traces of APs recorded from a representative myocyte in control conditions (black) and in the presence of 30 $\mu$M Phe (dark red). Insets show zoom-in of AP kickoff (Ci) and RMP (Cii). (Di) APD$_{50}$, (Dii) APD$_{80}$, (Diii) AP upstroke velocity, and (Div) AP amplitude. Significantly different from control, *$p < 0.05$, **$p < 0.01$, paired $t$-test, $n = 8$ cells from $N = 4$ hearts. Bars represent means $\pm$ SEMs. Numeric values are provided in Excel Table S2. Note: AP, action potential; APD$_{50}$, AP duration at 50% repolarization; APD$_{80}$, AP duration at 80% repolarization; dV/dt, upstroke velocity; RMP, resting membrane potential; SEM, standard error of the mean; TMC, time-matched control.

### Phe Exposure and K⁺ Channel Activity

Whole-cell voltage-clamp was used to record the main repolarizing currents of the murine myocardium; namely, inward rectifier potassium current ($I_{K1}$), transient outward ($I_{to}$), and ultrarapid delayed rectifier ($I_{Kur}$). Like all other species examined to date,[28,30,57,58] mouse $I_{K1}$, was not affected by Phe. $I_{K1}$ amplitude at $-60$ mV was $1.46 \pm 0.12$ pA/pF in control conditions and was $1.42 \pm 0.15$ pA/pF when maximally stimulated with 30 μM Phe ($n = 5$ cells from $N = 2$ hearts). Exposure to 1 μM Phe inhibited $I_{Kur}$, and exposure to 3, 10, and 30 μM Phe inhibited both $I_{to}$ and $I_{Kur}$ (Figure 3A,B; Kruskal–Wallis with Dunn's multiple comparisons test, $p < 0.01$ for all doses, $n = 6$–8 cells per group, $N = 5$ hearts for $I_{to}$, $N = 6$ hearts for $I_{Kur}$). Figure 3Ai and 3Bi show original traces of $I_{to}$ and $I_{Kur}$ recorded under control conditions and in the presence of 30 μM Phe, which decreased peak current amplitude by $37 \pm 4\%$ for $I_{to}$ ($p = 0.0001$) compared with control and by $53 \pm 5\%$ for $I_{Kur}$ ($p = 0.0001$). Absolute values for $I_{Kur}$ and $I_{to}$ current amplitude measured at each concentration are given in Table 2. These differences in outward K⁺ conductance could contribute to the APD prolongation seen in the myocytes. In addition to the suppression of peak current amplitude, Phe also affected the inactivation kinetics of $I_{Kur}$ and $I_{to}$ with acceleration of $I_{Kur}$ inactivation (Figure S3; repeated measures ANOVA, $p < 0.001$, $n > 6$ cells for each concentration).

### Phe Exposure and L-Type Ca²⁺ Channel Activity

The L-type Ca²⁺ current ($I_{Ca}$) is a key depolarizing current, which can drive changes in APD, particularly at 50% repolarization.[59] As shown in Figure 4, $I_{Ca}$ was significantly reduced upon Phe exposure at concentrations >3 μM, with maximum inhibition (38%) reached at 10 μM (Kruskal–Wallis with Dunn's multiple comparisons test, $p = 0.0221$ for 3 μM and $p = 0.0001$ for 10 and 30 μM, $n = 6$–10 cells per group, $N = 5$ hearts). The time course of $I_{CaL}$ inactivation (tau) was not affected by Phe: tau in milliseconds was $34.8 \pm 0.4$, $33.5 \pm 0.74$, $34.5 \pm 1.32$, $34.9 \pm 1.80$, $33.8 \pm 0.82$, and $38.3 \pm 1.43$ under control conditions and with 0.3, 1, 3, 10, and 30 μM Phe, respectively; $n = 6$–11 cells, from $N = 5$ hearts.

### Impact of Phe on the Sodium Current, $I_{Na}$, and Conduction Velocity

We evaluated the effects of Phe on $I_{Na}$ to understand whether the observed Phe-dependent reduction in upstroke velocity was due
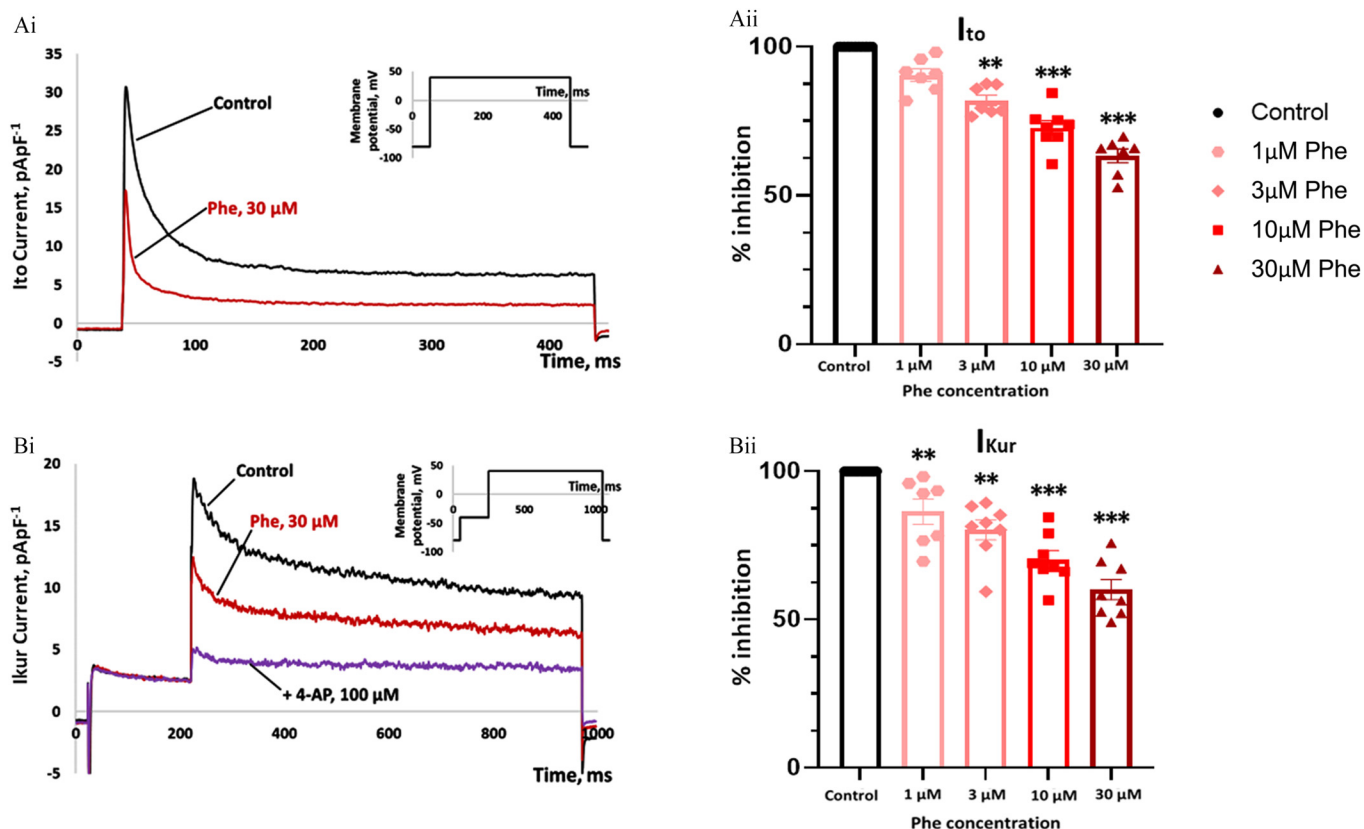


**Figure 3.** Effect of phenanthrene (Phe) on the transient outward potassium current ($I_{to}$) and the ultrarapid potassium current ($I_{Kur}$) in isolated murine ventricular myocytes. (Ai) Original traces of $I_{to}$ recorded from a representative myocyte in control conditions (black) and in the presence of 30 μM Phe (dark red). The current was induced by repetitive square-pulse depolarization from the holding potential of $-80$ mV to $+40$ mV, as shown in the inset. The $I_{to}$ amplitude was calculated as the difference between peak outward current value and the current measured at the end of the depolarizing square-pulse. (Aii) Relative magnitude of inhibitory effect on the amplitude of $I_{to}$ produced by 1–30 μM Phe. Significantly different from control, **$p < 0.001$, ***$p < 0.0001$, one-way ANOVA on ranks with Dunn's multiple comparisons test, $n = 7$–8 cells from $N = 5$ hearts. (Bi) Original traces of $I_{Kur}$ recorded from a representative myocyte in control conditions (black), in the presence of 30 μM Phe (dark red), and after addition of the $I_{Kur}$ blocker, 100 μM 4-aminopyridine (4-AP, purple). The current was induced by repetitive two-step depolarization from the holding potential of $-80$ mV to $-40$ mV (first step required for inactivation of $I_{Na}$ and $I_{to}$) and further to $+40$ mV (second step), as shown in the inset. $I_{Kur}$ amplitude was calculated as the difference between peak outward current before and after application of 100 μM 4-aminopyridine. (Bii) Relative magnitude of the inhibitory effect on the amplitude of $I_{Kur}$ produced by 1–30 μM Phe. Significantly different from control, **$p < 0.001$, ***$p < 0.0001$, one-way ANOVA on ranks with Dunn's multiple comparisons test, from $n = 7$–8 cells and $N = 6$ hearts. Bars represent means ± SEMs and points represent individual cells. Absolute peak current data for each current under control conditions and with each dose of Phe are given in Table 2. Note: %, percentage; ANOVA, analysis of variance; $I_{Na}$, fast sodium current; pA·pF⁻¹, current amplitude was normalized to cell capacitance; SEM, standard error of the mean.
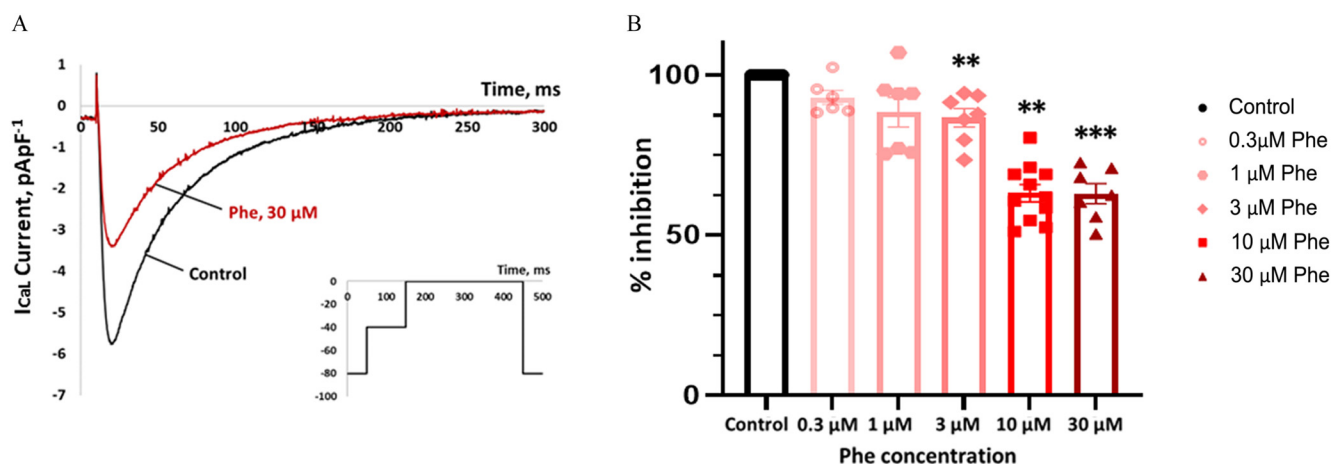
**Figure 4.** Effect of phenanthrene (Phe) on the L-type calcium current ($I_{Ca}$) in isolated murine ventricular myocytes. (A) Original traces of $I_{CaL}$ recorded from a representative myocyte in control conditions (black) and in the presence of 30 μM Phe (dark red). The current was induced by repetitive square-pulse two-step depolarization from the holding potential of $-80$ mV to $-40$ mV (first step required for inactivation of $I_{Na}$) and further to 0 mV (second step), as shown in the inset. (B) Relative magnitude of the inhibitory effect on $I_{CaL}$ produced by 0.3–30 μM Phe. The value of the Phe-resistant current is expressed as a percentage of control current amplitude. Significantly different from control, $^{**}p < 0.001$, $^{***}p < 0.0001$, one-way ANOVA on ranks with Dunn's multiple comparisons test, $n = 6–10$ cells and $N = 5$ hearts. Bars represent means ± SEMs and points represent individual cells. Absolute peak current data under control conditions and with each dose of Phe are given in Table 2. Note: %, percentage; ANOVA, analysis of variance; $I_{Na}$, fast sodium current; pA·pF$^{-1}$, current amplitude was normalized to cell capacitance; SEM, standard error of the mean.

to $I_{Na}$ inhibition. Figure 5Ai shows the original traces of $I_{Na}$ in control conditions and after exposure to 30 μM Phe. Significant inhibition was observed at 1 μM ($p = 0.036$), 3 μM ($p = 0.002$), 10 μM ($p = 0.0001$), and 30 μM ($p = 0.001$) Phe (Kruskal–Wallis with Dunn's multiple comparisons test, $n = 6–8$ cells per group, $N = 4$ hearts), with $36.7 \pm 4.7\%$ inhibition from control observed in the presence of 30 μM Phe. The time course of $I_{Na}$ inactivation (tau; $\tau_{fast}$ and $\tau_{slow}$) were not affected by Phe. $\tau_{fast}$ in milliseconds was $0.85 \pm 0.08$, $0.99 \pm 0.15$, $1.05 \pm 0.17$, $0.78 \pm 0.12$, and $0.59 \pm 0.1$, and $\tau_{slow}$ in milliseconds was $2.45 \pm 0.18$, $2.56 \pm 0.29$, $2.64 \pm 0.21$, $2.98 \pm 0.25$, and $2.06 \pm 0.33$ under control conditions and with 0.3, 1, 3, 10, and 30 μM Phe, respectively; $n = 6–7$ cells, from $N = 4$ hearts.

Inhibition of $I_{Na}$ could have a profound impact on conduction of the electrical signal across the heart. To investigate this, electrical activation maps were recorded from isolated murine ventricles before and after exposure to ~8 μM Phe. Representative electrical maps (Figure 5B), show slowing of the electrical wave following exposure to ~8 μM Phe resulting in a 42% reduction in ventricular conduction velocity (Figure 5C; two-way ANOVA mixed-effects analysis, $p = 0.0143$, $N = 7$ hearts).

### *Arrhythmia Susceptibility following Phe Exposure*

To investigate whether the Phe-induced change in conduction velocity and ion channel repolarization increased arrhythmia susceptibility, we used PES S1S2 pacing to induce ventricular arrhythmias in isolated murine hearts. Figure 6A shows a heart in normal rhythm in a time-matched control following PES and induction of VT in an ~8 μM Phe-exposed heart (raw ECG traces collected during the final stimulation interval). Of the hearts treated with ~8 μM Phe, 55% developed monomorphic VT in contrast to only 11% in the time-matched control hearts (Figure 6Bi; chi-square, $p = 0.0455$, $N = 9$ hearts). No spontaneous arrhythmias were observed during normal (non-PES) perfusion. To compare the severity of VT, all hearts were given an arrhythmia score (based on a published scoring method[53,54]; Table 1). The arrhythmia score was more than doubled in ~8 μM Phe-exposed hearts compared with control hearts, suggesting not only more VT, but also more severe VT, during Phe

exposure. There was no difference in ERP between control and exposed hearts ($0.03 \pm 0.01$ s for Phe and $0.04 \pm 0.02$ s for control, $p = 0.08$, $N = 7–8$).

### *Modeling the Impact of Phe Exposure on Human AP Duration*

To improve extrapolation from mouse to human, we used estimations of IC$_{50}$, n(H), and maximal block (Table S1) based on fractional block calculations for $I_{to}$, $I_{Ca}$, and $I_{Na}$ densities (Table 2) together with prior published potency against hERG[46] to estimate the impact of Phe on the human ventricular AP using an online modeling tool (see Figure 7). Although an approximation (see the "Materials and Methods" section for assumptions), the modeling revealed the potential for APD prolongation at nanomolar levels found in human serum.[40] For example, the model produced an ~10% prolongation of APD$_{90}$ at 0.3 μM of Phe (Figure 7 and Table S2).

### Discussion

The acute toxicity of the anthropogenic pollutant Phe on the mammalian heart was investigated *ex vivo* using a healthy mouse model. To our knowledge, we have shown increased arrhythmia susceptibility in response to Phe exposure for the first time in any species. The increased arrhythmia incidence in the mouse heart likely resulted from bradycardia, APD prolongation, and slowed conduction. We also showed that whole-heart effects were mediated by the inhibition of repolarizing K$^+$ currents and depolarizing Ca$^{2+}$ and Na$^+$ currents. The whole-heart effects were seen only at the higher dose applied (~8 μM). Although this concentration is greater than has been observed in human serum (3.3 μM),[40] because cardiotoxicity of air pollution is related to the exposure duration,[60] we would expect impacts at lower doses with longer exposures times (i.e., in excess of the 15 min employed here). Individual ion channel current effects were observed at 1 μM for $I_{Na}$, and at 3 μM for Ca$^{2+}$ and K$^+$ conductances. Moreover, when we input the ion current blocking potency data reported here for the mouse with previous work on hERG[46] into a human ventricular AP modeling tool, we observed APD prolongation at nanomolar concentrations of Phe exposure
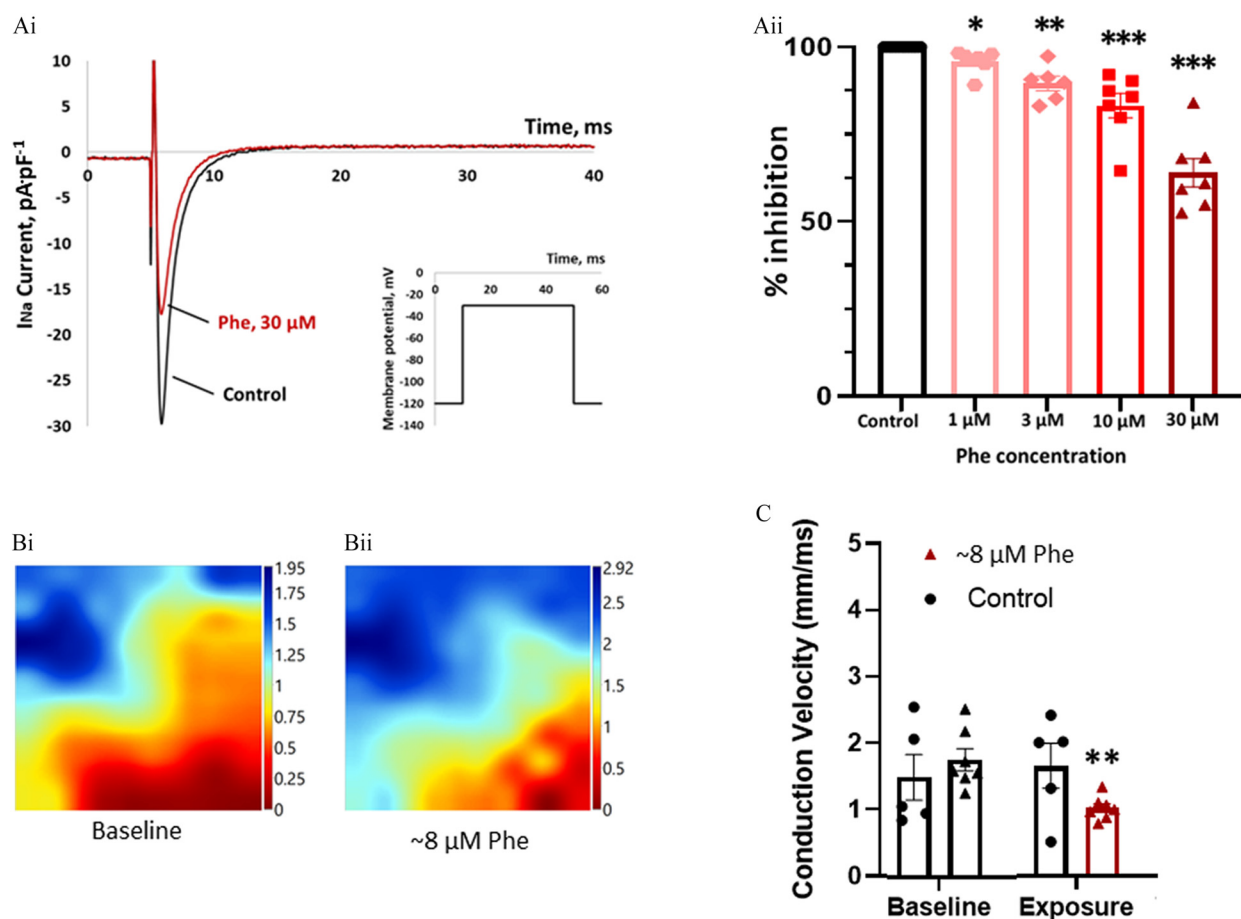
**Figure 5.** Effect of phenanthrene (Phe) on the fast sodium current $I_{Na}$ in murine ventricular myocytes and conduction velocity across the murine ventricle. (A). Impact of Phe on $I_{Na}$ in isolated murine ventricular myocytes. (Ai) Original traces of $I_{Na}$ recorded from a representative myocyte in control conditions (black) and in the presence of 30 μM Phe (dark red). The current was induced by repetitive square-pulse depolarization from the holding potential of −120 mV to −30 mV (maximum of I–V curve), shown in the inset. (Aii) Relative magnitude of the inhibitory effect on $I_{Na}$ produced by 1–30 μM Phe. The value of the Phe-resistant current is expressed as a percentage of control current magnitude. Significantly different from control, $^*p < 0.05$, $^{**}p < 0.01$, $^{***}p < 0.001$, one-way ANOVA on ranks with Dunn's multiple comparisons test, $n = 6$–7 cells and $N = 4$ hearts. Bars represent means ± SEMs and points represent individual cells. Absolute peak current data under control conditions and with each dose of Phe are given in Table 2. (B,C) The impact of Phe on cardiac conduction velocity in isolated murine hearts. (B) Representative electrical activation map from isolated hearts at baseline (Bi) and after exposure to ∼8 μM Phe. Each map illustrates the activation time across 64 channels, with red indicating the earliest activation point and blue the latest, scale represents time in milliseconds. The difference in activation time between the earliest and latest points was used to calculate the conduction velocity across the ventricle. (C) Ventricular conduction velocity (mm/ms) from isolated hearts exposed to either control solution (TMC is denoted by triangle symbols) or ∼8 μM Phe (dark red). Significantly different from baseline, $^{**}p < 0.01$, mixed-effects analysis with Tukey's multiple comparison test, $N = 5$–7 hearts. Bars represent means ± SEMs, with points representing individual hearts. Numeric values for conduction velocity are provided in Excel Table S3. Note: %, percentage; ANOVA, analysis of variance; pA·pF$^{-1}$, current amplitude was normalized to cell capacitance; SEM, standard error of the mean; TMC, Time-Matched Control.

(Figure 7 and Table S2). Collectively, our findings suggest that excitation–contraction coupling in the cardiomyocytes of healthy hearts are compromised by Phe at levels that exist currently in ambient air pollution[39,40] but that whole-heart dysfunction in the form of arrhythmias occurs at higher levels. These data present a clear warning for cardiovascular health, even in healthy individuals living in regions with poor air quality or in areas where spikes in poor air quality occur. It is also likely that the impact of Phe is more deleterious in individuals with underlying cardiac conditions.

### *Phe Prolongs Cardiac AP Duration through Inhibition of Repolarizing K⁺ Currents*

We observed a reduction in HR and a prolongation of PR interval, following Phe exposure at ∼8 μM; however, we observed no impact on other ECG parameters at this dose (Figure 1D and Figure S1) or on any parameter at the lower dose of ∼2.1 μM (Figure 1). A reduction in HR can manifest as bradycardia, a

common precursor for ventricular arrhythmias, including VT.[61] The PR interval represents conduction of the electrical signal from the atria to the ventricles and significant prolongation of the PR interval can underlie AV conduction block[62–64] and is pro-arrhythmic. Incardona et al. found a significant reduction in HR[24] and AV conduction block following Phe exposure in embryonic zebrafish,[26] consistent with our findings in mouse hearts. Whole-heart Phe exposure in adult fish caused prolongation of the QTc interval and ventricular MAPD,[27,30] an effect not resolvable in the present study despite the trend. However, in line with previous work in fish, we did observe APD prolongation at the cellular level at both 50% and 80% repolarization (Figure 2D).

AP prolongation is caused by an increase in depolarizing currents or a decrease in repolarizing currents. The AP prolongation observed here is likely derived from the latter effect driven by inhibition of $I_{to}$ and $I_{Kur}$ currents (Figure 3). To our knowledge, this is the first description of $I_{to}$ and $I_{Kur}$ inhibition by Phe and shows that, despite the lack of the $I_{Kr}$ current in the mouse,[65] AP prolongation still occurred. Similar to a previous
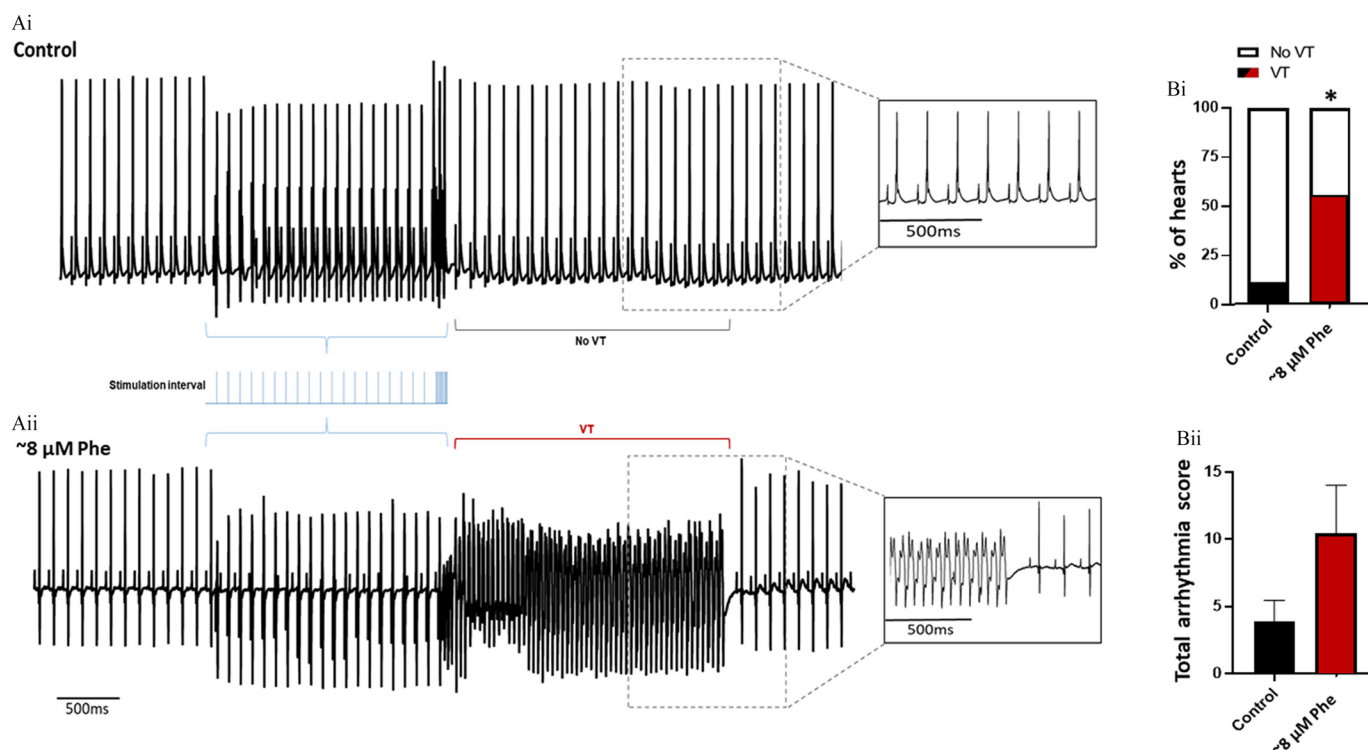
**Figure 6.** Effect of phenanthrene (Phe) on arrhythmia susceptibility following programmed electrical stimulation in mouse heart. (A) Representative ECG recordings from control (Ai) and ~ 8 μM Phe-exposed (Aii) hearts. Blue brackets indicate the final interval of the programmed electrical stimulation protocol, with the blue inset showing each extra-stimulus beat. The red bracket highlights the induction of ventricular tachycardia (VT) in the Phe-exposed heart, with the black bracket showing regular rhythm during the same period in a control heart. Insets show zoom-in of VT/No VT segment. VT was defined as >4 premature ventricular complexes. (B) Quantification of arrhythmia susceptibility following acute Phe exposure. (Bi) Percentage of hearts that developed VT in control (black) and Phe-exposed (dark red) hearts. Bars represent total number of hearts tested, with the shaded area indicating VT. (Bii) Arrhythmia susceptibility score,[50] in control (black) and ~ 8 μM Phe-exposed (dark red) hearts. The higher the score the more severe the arrhythmic phenotype. Bars represent means ± SEMs. Significantly different from control, $^*p < 0.05$, chi-square test, $N = 9$ hearts. Numeric values for arrhythmic induction and arrhythmic score are provided in Excel Table S4. Note: ECG, electrocardiography.

study in zebrafish,[28] the gating kinetics of both repolarizing $K^+$ currents in the mouse ventricle were modified with an increase in $I_{to}$ and $I_{Kur}$ inactivation that could exacerbate the reduction in charge transferred through these channels during an AP (Figure S3). This is worrisome for human cardiac health given that previous studies have linked changes in $K^+$ conductance and APD prolongation to ventricular arrhythmias, including torsades de pointes.[66,67] In humans, $I_{to}$[68] and $I_{Kur}$[69] have been associated with atrial fibrillation. $I_{to}$ in both the mouse and the human is carried by Kv4.3, and in heart failure[70] and chronic atrial fibrillation, $I_{to}$ is markedly reduced and Kv4.3 down-regulated.[68,71] The effect of Phe on atrial repolarization was not investigated in this study but future work here would help determine the impact of exposure on human atrial function. Indeed, the clinical significance of $I_{to}$ inhibition observed here is highlighted by the association between mutations in the gene encoding Kv4.3 (*KCND3*) and cases of Brugada syndrome,[72,73] familial atrial fibrillation,[74,75] early repolarization syndrome,[76] and sudden unexplained death.[77]

We also show inhibition of $I_{CaL}$ by Phe in the mouse ventricle (Figure 4), and although this has been shown previously in fish,[28,30] this is the first report we know of in mammals. Inhibition of $I_{CaL}$ is most often linked to AP shortening, not prolongation, and may contribute to the lack of APD prolongation at the whole-heart level. A recent study in zebrafish showed APD shortening despite significant inhibition of $I_{Kr}$ due to potency on $I_{CaL}$.[28] A reduction in the amplitude of $I_{CaL}$ would result in APD shortening at 50% repolarization (APD$_{50}$), and this may explain the lack of overall effect of Phe on APD in the lower dose range. However, at 30 μM, APD prolongation was seen at both 50% and 80% repolarization likely owing to the large

impact of Phe on the outward $K^+$ currents at this dose and the lesser contribution of $I_{CaL}$ to depolarizing current in mouse AP generation.[78,79] Indeed, potency of $I_{Kr}$ inhibition is important for APD characteristics as demonstrated by computational data for the human ventricular APD response to Phe exposure provided in Figure 7.

### Inhibition of $I_{Na}$ by Phe Results in Slowed Ventricular Conduction

There is a large focus in the literature on Phe and repolarizing currents; however, a recent study in fish pointed to inhibitory effects on the inward $I_{Na}$ current.[29] In mice, similar to in humans, the influx of $Na^+$ through voltage-gated sodium channels drives the upstroke of the ventricular AP and is responsible for AP initiation and propagation.[80] We found significant inhibition of $I_{Na}$ (Figure 5A), even at the lower end of the Phe concentration range tested, resulting in reduced AP upstroke velocity (Figure 2Diii) and reduced AP amplitude (Figure 2iv). Inhibition of $I_{Na}$ and the associated changes in AP morphology are known to be pathological because these changes can impair the synchronous and rapid conduction of electrical activity across the heart,[80,81] increasing the risk of arrhythmias.[82–84] Accordingly, we showed reduced conduction velocity following Phe exposure at the whole-heart level for the first time to our knowledge in any species (Figure 5B), raising the possibility of reentrant arrhythmias as a mechanism for Phe cardiotoxicty.[84–86] Indeed, the PR interval prolongation following acute Phe exposure in this study could be indicative of first-degree AV block, where a 1:1 ratio of P wave to QRS wave is maintained. Moreover, previous work with PM and diesel particles have been
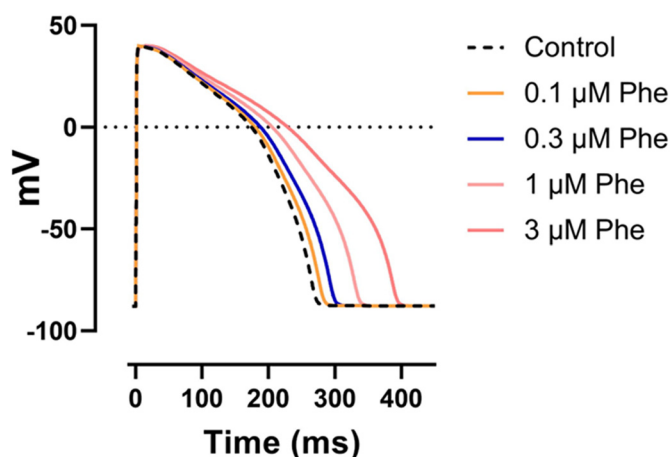
**Figure 7.** Computational model showing effect of phenanthrene (Phe) on human ventricular action potential (AP). We estimated the impact of Phe on the human ventricular AP through *in silico* modeling using calculations of $IC_{50}$, n(H), and maximal block (Table S1) based on fractional block estimated from murine $I_{to}$, $I_{Ca}$, and $I_{Na}$ densities (Table 2) and $I_{Kr}$ calculated from hERG1a/1b[46] in the place of the place of murine $I_{Kur}$. Note the 10% prolongation of $APD_{90}$ at 0.3 μM of Phe, which is found in human serum.[40] See Table S2 for impact of Phe on other tabulated AP parameters. AP simulations were conducted using the online Action Potential–Portal prediction software.[56,104] Note: $APD_{90}$, action potential duration at 90% repolarization; $IC_{50}$, 50% inhibitory concentration; $I_{Ca}$, calcium current; $I_{Kr}$, native potassium current; $I_{Kur}$, ultrarapid potassium current; $I_{Na}$, fast sodium current; $I_{to}$, transient outward potassium current.

shown to slow conduction velocity and induce arrhythmia in rodents.[87,88]

Knowing the Phe (or PAH) contribution in studies such as these would be instructive for improving our understanding of the mechanism of toxicity. A synthesized derivative of Phe, 9-phenanthrol has also recently been shown to block peak and late $Na^+$-channels in the rabbit heart.[89] Overall, we showed changes in $I_{Na}$, AP upstroke velocity, and AP amplitude in the cardiomyocyte, which manifested as differences in whole-heart cardiac electrical activity following Phe exposure in the mouse. Thus, we have shown here that the pro-arrhythmic phenotype brought about by altered ventricular repolarization following Phe exposure is compounded by the Phe-induced reduction in conduction velocity.

### *Phe Increases Arrhythmia Susceptibility*

Bradycardia and reduced conduction velocity, combined with the cellular changes in AP morphology and ion flux reported here, point to a pro-arrhythmic phenotype following Phe exposure. Previous studies in fish have shown similar cellular effects and alluded to a pro-arrhythmic effect of Phe exposure; however, no study to date has conclusively linked Phe exposure to arrhythmogenesis. VT is a commonly occurring and potentially life-threatening arrhythmia, caused by abnormal electrical activity of the ventricle.[90,91] Here we showed a significant increase in the incidence of VT induction in Phe-treated hearts (Figure 6). Paired with the observed increase in arrhythmia score (Figure 6Bii), these data suggest that Phe directly increased arrhythmia susceptibility.

Epidemiological evidence has long shown a positive association between $PM_{2.5}$ concentration and the incidence of arrhythmias[14] and both PM and diesel particles have been shown to trigger arrhythmia in rodents.[87,88] Our findings suggest Phe could be involved in these pathologies. VT and ventricular fibrillation are the primary causes of arrhythmia-induced sudden cardiac death[92] and the increased incidence of VT described here using mouse hearts could contribute to the increased incidence of sudden cardiac death in areas of high

$PM_{2.5}$ exposure. Slowed conduction and AP prolongation in the ventricle are common substrates associated with the induction of VT.[92] Bradycardia is also associated with early after depolarizations (EADs), and increased frequency of EADs can act as a trigger for VT induction.[92] Finally, the effects of Phe described above for key ion currents could act as triggers and substrates for VT induction and maintenance.[92–94] Reduced $I_{Na}$ density and accelerated inactivation have been linked to ventricular arrhythmias, particularly in relation to conduction failure.[95] Indeed the increased VT susceptibility seen with Phe exposure in this investigation was primarily monomorphic VT, and therefore the reductions in $I_{Na}$ and subsequent slowed conduction velocity were likely the dominant mechanisms driving the arrhythmia, possibly via reentrant-based mechanisms.[96] The pro-arrhythmic phenotype shown here *ex vivo* for mice could be exacerbated by underlying electrical impairment. If similar mechanisms apply in humans, then arrhythmia could be expected to be more prominent in patients with significant scarring following myocardial infarction, which acts as a substrate for monomorphic VT.

### *Study Limitations and Considerations*

To our knowledge, for the first time in mammals, we show that the air pollutant Phe inhibited ionic conductances ($I_{Na}$, $I_{Ca}$, $I_{to}$, and $I_{Kur}$) key for cardiac excitation–contraction coupling, resulting in prolonged cellular AP, slowed conduction, and increased arrhythmic potential in an *ex vivo* mouse heart model. The mechanisms of channel inhibition, however, remain to be elucidated. Our previous work with recombinant hERG channels expressed in HEK293 cells showed Phe acted as a direct inhibitor interacting with the hERG channel, binding to a distinct site in the channel pore domain.[46] Whether the murine channels identified here are also inhibited by direct block await mutagenesis-inhibition studies. However, based on a number of observations, we suspect the block we observed is specific rather than a secondary effect of nonspecific membrane disruption. First, here and in our previous work with native cardiomyocytes from a range of species,[28–30] we observed no change in cell impedance assessed via voltage-clamp parameters that would be expected if membranes were disrupted following exposure. We also showed Phe exposure impacted some but not all ion channel function, which would be unexpected if it were affecting channels indirectly via membrane disruption.[28] Similarly, we showed that inactivation kinetics of some ($I_{to}$ and $I_{Kur}$) but not all ($I_{Ca}$ and $I_{Na}$) channels were impacted by exposure (Figure S3). Thus, although Phe will accumulate in fat,[45] we do not believe the cardiotoxicity demonstrated here can be attributed simply to nonspecific membrane disruption.

However, we do acknowledge the probable contribution of other toxicity pathways in the observed responses. As demonstrated in various human cell types[97] and urine analysis of coke oven workers,[98] exposure to air pollution induces inflammation and oxidative stress, leading to damage of DNA, lipids, and proteins.[99] Indeed, acute inhalation of nanoparticles induced cardiac arrhythmias and slow conduction velocity in rats, and this was associated with an increase in lipid peroxidation markers in lung and cardiac tissue.[100,101] Reactive oxygen species (ROS) can also act directly on ion channels[102] with exogenous ROS attenuating $I_{Ca}$ in guinea pig ventricular myocytes.[103] Undoubtably, air pollution and the PAHs contained within, produce their toxic effects through a multitude of pathways. Future work should investigate the degree to which Phe activates oxidative stress and inflammation pathways in both acute and chronic scenarios to better delineate the role they play in pollution-induced cardiotoxicity.

### Conclusions

In the present study, we have shown that exposure to a single but ubiquitous pollutant, Phe, directly altered the electrical activity of

the mouse heart in an *ex vivo* model, providing, to our knowledge, the first evidence directly linking Phe exposure to increased arrhythmia susceptibility in mammals. We also provide what we believe to be the first evidence of Phe inhibiting $I_{to}$ and $I_{Kur}$ along with $I_{Na}$ in a concentration-dependent manner leading to prolongation of the AP, bradycardia, and slowing of conduction velocity. These proarrhythmic ionic mechanisms could be targeted to manage and mitigate morbidity. Air pollution contains Phe in both the gas phase and adsorbed to $PM_{2.5}$ and thus our study provides a possible mechanism linking poor air quality to previous work on rodents[87,88] and with human cardiac health risk. Like other risk factors, such as poor diet, low physical activity, and smoking,[2,11,13] clinicians should include air pollution as an aggravating factor in cardiovascular disease screening. Patients with underlying conditions who live in areas with high atmospheric Phe levels, should be warned of the dangers this poses to their health. As global levels of pollution rise, and more people move to urban areas, the *ex vivo* cardiotoxicity in mice reported here may serve as a warning sign for the cardiovascular well-being of humans. Future studies focusing on the chronic effects of low level Phe exposure are needed to improve current extrapolations to the human health perspective.

## Acknowledgments

## References

1. GBD 2019 Risk Factors Collaborators. 2020. Global burden of 87 risk factors in 204 countries and territories, 1990–2019: a systematic analysis for the Global Burden of Disease Study 2019. Lancet 396(10258):1223–1249, PMID: 33069327, https://doi.org/10.1016/S0140-6736(20)30752-2.
2. Lelieveld J, Klingmüller K, Pozzer A, Pöschl U, Fnais M, Daiber A, et al. 2019. Cardiovascular disease burden from ambient air pollution in Europe reassessed using novel hazard ratio functions. Eur Heart J 40(20):1590–1596, PMID: 30860255, https://doi.org/10.1093/eurheartj/ehz135.
3. Lee KK, Miller MR, Shah ASV. 2018. Air pollution and stroke. J Stroke 20(1):2–11, PMID: 29402072, https://doi.org/10.5853/jos.2017.02894.
4. Cohen AJ, Brauer M, Burnett R, Anderson HR, Frostad J, Estep K. 2018. Estimates and 25-year trends of the global burden of disease attributable to ambient air pollution: an analysis of data from the Global Burden of Diseases Study 2015 [389(10082):1907–2018] [Erratum]. Lancet 391(10130):1576, PMID: 28408086, https://doi.org/10.1016/S0140-6736(17)30505-6.
5. Aung N, Sanghvi MM, Zemrak F, Lee AM, Cooper JA, Paiva JM, et al. 2018. Association between ambient air pollution and cardiac morpho-functional phenotypes insights from the UK Biobank Population Imaging Study. Circulation 138(20):2175–2186, PMID: 30524134, https://doi.org/10.1161/CIRCULATIONAHA.118.034856.
6. Poursafa P, Moosazadeh M, Abedini E, Hajizadeh Y, Mansourian M, Pourzamani H, et al. 2017. A systematic review on the effects of polycyclic aromatic hydrocarbons on cardiometabolic impairment. Int J Prev Med 8:19, PMID: 28479961, https://doi.org/10.4103/ijpvm.IJPVM_144_17.
7. Atkinson RW, Carey IM, Kent AJ, van Staa TP, Anderson HR, Cook DG. 2013. Long-term exposure to outdoor air pollution and incidence of cardiovascular diseases. Epidemiology 24(1):44–53, PMID: 23222514, https://doi.org/10.1097/EDE.0b013e318276ccb8.
8. Ritchie H, Roser M. 2021. Air Pollution. *OurWorldInData*. [Online Resource.] https://ourworldindata.org/air-pollution [accessed 5 May 2023].
9. WHO (World Health Organization). 2019. 05-03-19 ed. https://www.who.int/ [accessed 5 May 2023].
10. WHO. 2018. Air pollution levels rising in many of the world's poorest cities. https://www.who.int/news-room/headlines/12-05-2016-air-pollution-levels-rising-in-many-of-the-world-s-poorest-cities [accessed 2 July 2020].
11. Pope CA III, Burnett RT, Thurston GD, Thun MJ, Calle EE, Krewski D, et al. 2004. Cardiovascular mortality and long-term exposure to particulate air pollution—epidemiological evidence of general pathophysiological pathways of disease. Circulation 109(1):71–77, PMID: 14676145, https://doi.org/10.1161/01.CIR.0000108927.80044.7F.
12. Pope CA III, Burnett RT, Thun MJ, Calle EE, Krewski D, Ito K, et al. 2002. Lung cancer, cardiopulmonary mortality, and long-term exposure to fine particulate air pollution. JAMA 287(9):1132–1141, PMID: 11879110, https://doi.org/10.1001/jama.287.9.1132.
13. Brook RD, Rajagopalan S, Pope CA III, Brook JR, Bhatnagar A, Diez-Roux AV, et al. 2010. Particulate matter air pollution and cardiovascular disease: an update to the scientific statement from the American Heart Association. Circulation 121(21):2331–2378, PMID: 20458016, https://doi.org/10.1161/CIR.0b013e3181dbece1.
14. Franklin BA, Brook R, Pope CA III. 2015. Air pollution and cardiovascular disease. Curr Probl Cardiol 40(5):207–238, PMID: 25882781, https://doi.org/10.1016/j.cpcardiol.2015.01.003.
15. Miller MR, Newby DE. 2020. Air pollution and cardiovascular disease: *car sick*. Cardiovasc Res 116(2):279–294, PMID: 31583404, https://doi.org/10.1093/cvr/cvz228.
16. Newby DE, Mannucci PM, Tell GS, Baccarelli AA, Brook RD, Donaldson K, et al. 2015. Expert position paper on air pollution and cardiovascular disease. Eur Heart J 36(2):83–93b, PMID: 25492627, https://doi.org/10.1093/eurheartj/ehu458.
17. Delfino RJ, Sioutas C, Malik S. 2005. Potential role of ultrafine particles in associations between airborne particle mass and cardiovascular health. Environ Health Perspect 113(8):934–946, PMID: 16079061, https://doi.org/10.1289/ehp.7938.
18. Niemann B, Rohrbach S, Miller MR, Newby DE, Fuster V, Kovacic JC. 2017. Oxidative stress and cardiovascular risk: obesity, diabetes, smoking, and pollution: part 3 of a 3-part series. J Am Coll Cardiol 70(2):230–251, PMID: 28683970, https://doi.org/10.1016/j.jacc.2017.05.043.
19. Marris CR, Kompella SN, Miller MR, Incardona JP, Brette F, Hancox JC, et al. 2020. Polyaromatic hydrocarbons in pollution: a heart-breaking matter. J Physiol 598(2):227–247, PMID: 31840250, https://doi.org/10.1113/JP278885.
20. Ito K, Mathes R, Ross Z, Nádas A, Thurston G, Matte T. 2011. Fine particulate matter constituents associated with cardiovascular hospitalizations and mortality in New York City. Environ Health Perspect 119(4):467–473, PMID: 21463978, https://doi.org/10.1289/ehp.1002667.
21. Elliott EG, Laden F, James P, Rimm EB, Rexrode KM, Hart JE. 2020. Interaction between long-term exposure to fine particulate matter and physical activity, and risk of cardiovascular disease and overall mortality in U.S. women. Environ Health Perspect 128(12):127012, PMID: 33356515, https://doi.org/10.1289/EHP7402.
22. Donaldson K, Duffin R, Langrish JP, Miller MR, Mills NL, Poland CA, et al. 2013. Nanoparticles and the cardiovascular system: a critical review. Nanomedicine (Lond) 8(3):403–423, PMID: 23477334, https://doi.org/10.2217/nnm.13.16.
23. Miller MR, Shaw CA, Langrish JP. 2012. From particles to patients: oxidative stress and the cardiovascular effects of air pollution. Future Cardiol 8(4):577–602, PMID: 22871197, https://doi.org/10.2217/fca.12.43.
24. Incardona JP, Collier TK, Scholz NL. 2004. Defects in cardiac function precede morphological abnormalities in fish embryos exposed to polycyclic aromatic hydrocarbons. Toxicol Appl Pharmacol 196(2):191–205, PMID: 15081266, https://doi.org/10.1016/j.taap.2003.11.026.
25. Incardona JP, Carls MG, Teraoka H, Sloan CA, Collier TK, Scholz NL. 2005. Aryl hydrocarbon receptor-independent toxicity of weathered crude oil during fish development. Environ Health Perspect 113(12):1755–1762, PMID: 16330359, https://doi.org/10.1289/ehp.8230.
26. Incardona JP, Carls MG, Day HL, Sloan CA, Bolton JL, Collier TK, et al. 2009. Cardiac arrhythmia is the primary response of embryonic Pacific herring (*Clupea pallasi*) exposed to crude oil during weathering. Environ Sci Technol 43(1):201–207, PMID: 19209607, https://doi.org/10.1021/es802270t.
27. Brette F, Shiels HA, Galli GLJ, Cros C, Incardona JP, Scholz NL, et al. 2017. A novel cardiotoxic mechanism for a pervasive global pollutant. Sci Rep 7:41476, PMID: 28139666, https://doi.org/10.1038/srep41476.
28. Kompella SN, Brette F, Hancox JC, Shiels HA. 2021. Phenanthrene impacts zebrafish cardiomyocyte excitability by inhibiting IKr and shortening action potential

duration. J Gen Physiol 153(2):e202012733, PMID: 33475719, https://doi.org/10.1085/jgp.202012733.

29. Abramochkin DV, Kompella SN, Shiels HA. 2021. Phenanthrene alters the electrical activity of atrial and ventricular myocytes of a polar fish, the Navaga cod. Aquat Toxicol 235:105823, PMID: 33906022, https://doi.org/10.1016/j.aquatox.2021.105823.

30. Ainerua MO, Tinwell J, Kompella SN, Sørhus E, White KN, van Dongen BE, et al. 2020. Understanding the cardiac toxicity of the anthropogenic pollutant phenanthrene on the freshwater indicator species, the brown trout (*Salmo trutta*): from whole heart to cardiomyocytes. Chemosphere 239:124608, PMID: 31499312, https://doi.org/10.1016/j.chemosphere.2019.124608.

31. Ainerua MO, Tinwell J, Murphy R, Galli GLJ, van Dongen BE, White KN, et al. 2021. Prolonged phenanthrene exposure reduces cardiac function but fails to mount a significant oxidative stress response in the signal crayfish (*Pacifastacus leniusculus*). Chemosphere 268:129297, PMID: 33359987, https://doi.org/10.1016/j.chemosphere.2020.129297.

32. Brette F, Machado B, Cros C, Incardona JP, Scholz NL, Block BA. 2014. Crude oil impairs cardiac excitation-contraction coupling in fish. Science 343(6172):772–776, PMID: 24531969, https://doi.org/10.1126/science.1242747.

33. Abdel-Shafy HI, Mansour MSM. 2016. A review on polycyclic aromatic hydrocarbons: source, environmental impact, effect on human health and remediation. Egypt J Pet 25(1):107–123, https://doi.org/10.1016/j.ejpe.2015.03.011.

34. Schauer JJ, Kleeman MJ, Cass GR, Simoneit BRT. 1999. Measurement of emissions from air pollution sources. 2. $C_1$ through $C_{30}$ organic compounds from medium duty diesel trucks. Environ Sci Technol 33(10):1578–1587, https://doi.org/10.1021/es980081n.

35. Vu AT, Taylor KM, Holman MR, Ding YS, Hearn B, Watson CH. 2015. Polycyclic aromatic hydrocarbons in the mainstream smoke of popular U.S. cigarettes. Chem Res Toxicol 28(8):1616–1626, PMID: 26158771, https://doi.org/10.1021/acs.chemrestox.5b00190.

36. Liu Y, Zhu L, Shen X. 2001. Polycyclic aromatic hydrocarbons (PAHs) in indoor and outdoor air of Hangzhou, China. Environ Sci Technol 35(5):840–844, PMID: 11351525, https://doi.org/10.1021/es001354t.

37. Naumova YY, Eisenreich SJ, Turpin BJ, Weisel CP, Morandi MT, Colome SD, et al. 2002. Polycyclic aromatic hydrocarbons in the indoor and outdoor air of three cities in the U.S. Environ Sci Technol 36(12):2552–2559, PMID: 12099449, https://doi.org/10.1021/es015727h.

38. Tsapakis M, Stephanou EG. 2005. Occurrence of gaseous and particulate polycyclic aromatic hydrocarbons in the urban atmosphere: study of sources and ambient temperature effect on the gas/particle concentration and distribution. Environ Pollut 133(1):147–156, PMID: 15327865, https://doi.org/10.1016/j.envpol.2004.05.012.

39. Halsall CJ, Coleman PJ, Davis BJ, Burnett V, Waterhouse KS, Harding-Jones P, et al. 1994. Polycyclic aromatic hydrocarbons in U.K. urban air. Environ Sci Technol 28(13):2380–2386, PMID: 22176058, https://doi.org/10.1021/es00062a024.

40. Chrysochou E, Kanellopoulos PG, Koukoulakis KG, Sakellari A, Karavoltsos S, Minaidis M, et al. 2021. Heart failure and PAHs, OHPAHs, and trace elements levels in human serum: results from a preliminary pilot study in Greek population and the possible impact of air pollution. Molecules 26(11):3207, PMID: 34071927, https://doi.org/10.3390/molecules26113207.

41. Jacob J, Seidel A. 2002. Biomonitoring of polycyclic aromatic hydrocarbons in human urine. J Chromatogr B Analyt Technol Biomed Life Sci 778(1–2):31–47, PMID: 12376115, https://doi.org/10.1016/s0378-4347(01)00467-4.

42. Schober W, Pusch G, Oeder S, Reindl H, Behrendt H, Buters JTM. 2010. Metabolic activation of phenanthrene by human and mouse cytochromes P450 and pharmacokinetics in CYP1A2 knockout mice. Chem Biol Interact 183(1):57–66, PMID: 19766613, https://doi.org/10.1016/j.cbi.2009.09.008.

43. Carls MG, Rice SD, Hose JE. 1999. Sensitivity of fish embryos to weathered crude oil: part I. Low-level exposure during incubation causes malformations, genetic damage, and mortality in larval pacific herring (*Clupea pallasi*). Environ Toxicol Chem 18(3):481–493, https://doi.org/10.1002/etc.5620180317.

44. Wang Y, Zhu L, James-Todd T, Sun Q. 2022. Urinary polycyclic aromatic hydrocarbon excretion and regional body fat distribution: evidence from the U.S. National Health and Nutrition Examination Survey 2001–2016. Environ Health 21(1):75, PMID: 35945606, https://doi.org/10.1186/s12940-022-00890-8.

45. Mlyczyńska E, Bongrani A, Rame C, Węgiel M, Maślanka A, Major P, et al. 2023. Concentration of polycyclic aromatic hydrocarbons (PAHs) in human serum and adipose tissues and stimulatory effect of naphthalene in adipogenesis in 3T3-L1 cells. Int J Mol Sci 24(2):1455, PMID: 36674971, https://doi.org/10.3390/ijms24021455.

46. Al-Moubarak E, Shiels HA, Zhang Y, Du C, Hanington O, Harmer SC, et al. 2021. Inhibition of the hERG potassium channel by phenanthrene: a polycyclic aromatic hydrocarbon pollutant. Cell Mol Life Sci 78(23):7899–7914, PMID: 34727194, https://doi.org/10.1007/s00018-021-03967-8.

47. Incardona JP, Collier TK, Scholz NL. 2011. Oil spills and fish health: exposing the heart of the matter. J Expo Sci Environ Epidemiol 21(1):3–4, PMID: 21068721, https://doi.org/10.1038/jes.2010.51.

48. Huang L, Xi Z, Wang C, Zhang Y, Yang Z, Zhang S, et al. 2016. Phenanthrene exposure induces cardiac hypertrophy via reducing miR-133a expression by DNA methylation. Sci Rep 6:20105, PMID: 26830171, https://doi.org/10.1038/srep20105.

49. Ma H, Wang H, Zhang H, Guo H, Zhang W, Hu F, et al. 2020. Effects of phenanthrene on oxidative stress and inflammation in lung and liver of female rats. Environ Toxicol 35(1):37–46, PMID: 31456356, https://doi.org/10.1002/tox.22840.

50. Smith KEC, Dom N, Blust R, Mayer P. 2010. Controlling and maintaining exposure of hydrophobic organic compounds in aquatic toxicity tests by passive dosing. Aquat Toxicol 98(1):15–24, PMID: 20170970, https://doi.org/10.1016/j.aquatox.2010.01.007.

51. Mitchell GF, Jeron A, Koren G. 1998. Measurement of heart rate and Q-T interval in the conscious mouse. Am J Physiol 274(3):H747–H751, PMID: 9530184, https://doi.org/10.1152/ajpheart.1998.274.3.H747.

52. Curtis MJ, Hancox JC, Farkas A, Wainwright CL, Stables CL, Saint DA, et al. 2013. The Lambeth Conventions (II): guidelines for the study of animal and human ventricular and supraventricular arrhythmias. Pharmacol Ther 139(2):213–248, PMID: 23588158, https://doi.org/10.1016/j.pharmthera.2013.04.008.

53. Hayter EA, Wehrens SMT, Van Dongen HPA, Stangherlin A, Gaddameedhi S, Crooks E, et al. 2021. Distinct circadian mechanisms govern cardiac rhythms and susceptibility to arrhythmia. Nat Commun 12(1):2472, PMID: 33931651, https://doi.org/10.1038/s41467-021-22788-8.

54. Clasen L, Eickholt C, Angendohr S, Jungen C, Shin DI, Donner B, et al. 2018. A modified approach for programmed electrical stimulation in mice: inducibility of ventricular arrhythmias. PLoS One 13(8):e0201910, PMID: 30133474, https://doi.org/10.1371/journal.pone.0201910.

55. Isenberg G, Klockner U. 1982. Calcium tolerant ventricular myocytes prepared by preincubation in a "KB medium." Pflugers Arch 395(1):6–18, PMID: 7177773, https://doi.org/10.1007/BF00584963.

56. Williams G, Mirams GR. 2015. A web portal for in-silico action potential predictions. J Pharmacol Toxicol Methods 75:10–16, PMID: 25963830, https://doi.org/10.1016/j.vascn.2015.05.002.

57. Vehniäinen ER, Haverinen J, Vornanen M. 2019. Polycyclic aromatic hydrocarbons phenanthrene and retene modify the action potential via multiple ion currents in rainbow trout *Oncorhynchus mykiss* cardiac myocytes. Environ Toxicol Chem 38(10):2145–2153, PMID: 31237719, https://doi.org/10.1002/etc.4530.

58. Heuer RM, Galli GLJ, Shiels HA, Fieber LA, Cox GK, Mager EM, et al. 2019. Impacts of *Deepwater Horizon* crude oil on mahi-mahi (*Coryphaena hippurus*) heart cell function. Environ Sci Technol 53(16):9895–9904, PMID: 31343865, https://doi.org/10.1021/acs.est.9b03798.

59. Bers DM. 2002. Cardiac excitation–contraction coupling. Nature 415(6868):198–205, PMID: 11805843, https://doi.org/10.1038/415198a.

60. Grande G, Ljungman PLS, Eneroth K, Bellander T, Rizzuto D. 2020. Association between cardiovascular disease and long-term exposure to air pollution with the risk of dementia. JAMA Neurol 77(7):801–809, PMID: 32227140, https://doi.org/10.1001/jamaneurol.2019.4914.

61. Scherlag BJ, Kabell G, Harrison L, Lazzara R. 1982. Mechanisms of bradycardia-induced ventricular arrhythmias in myocardial ischemia and infarction. Circulation 65(7):1429–1434, PMID: 7074798, https://doi.org/10.1161/01.cir.65.7.1429.

62. Gehrmann J, Frantz S, Maguire CT, Vargas M, Ducharme A, Wakimoto H, et al. 2001. Electrophysiological characterization of murine myocardial ischemia and infarction. Basic Res Cardiol 96(3):237–250, PMID: 11403417, https://doi.org/10.1007/s003950170054.

63. Heijman J, Voigt N, Nattel S, Dobrev D. 2014. Cellular and molecular electrophysiology of atrial fibrillation initiation, maintenance, and progression. Circ Res 114(9):1483–1499, PMID: 24763466, https://doi.org/10.1161/CIRCRESAHA.114.302226.

64. Petrone G, Theodoropoulos P, Punjabi P. 2015. Cardiac Electrophysiology: From Cell to Bedside (sixth edition). 2014. [Book review.] Perfusion 30(5):431–432.

65. Nerbonne JM. 2004. Studying cardiac arrhythmias in the mouse—a reasonable model for probing mechanisms? Trends Cardiovasc Med 14(3):83–93, PMID: 15121155, https://doi.org/10.1016/j.tcm.2003.12.006.

66. Eisner DA, Dibb KM, Trafford AW. 2009. The mechanism and significance of the slow changes of ventricular action potential duration following a change of heart rate. Exp Physiol 94(5):520–528, PMID: 19270038, https://doi.org/10.1113/expphysiol.2008.044008.

67. Morissette P, Hreiche R, Turgeon J. 2005. Drug-induced long QT syndrome and torsade de pointes. Can J Cardiol 21(10):857–864, PMID: 16107909.

68. Grammer JB, Bosch RF, Kühlkamp V, Seipel L. 2000. Molecular remodeling of Kv4.3 potassium channels in human atrial fibrillation. J Cardiovasc Electrophysiol 11(6):626–633, PMID: 10868735, https://doi.org/10.1111/j.1540-8167.2000.tb00024.x.

69. Aguilar M, Feng J, Vigmond E, Comtois P, Nattel S. 2017. Rate-dependent role of $I_{Kur}$ in human atrial repolarization and atrial fibrillation maintenance. Biophys J 112(9):1997–2010, PMID: 28494969, https://doi.org/10.1016/j.bpj.2017.03.022.

70. Fowler ED, Wang N, Hezzell MJ, Chanoit G, Hancox JC, Cannell MB. 2022. Improved $Ca^{2+}$ release synchrony following selective modification of $I_{tof}$ and phase 1 repolarization in normal and failing ventricular myocytes. J Mol Cell Cardiol 172:52–62, PMID: 35908686, https://doi.org/10.1016/j.yjmcc.2022.07.009.

71. Workman AJ, Marshall GE, Rankin AC, Smith GL, Dempster J. 2012. Transient outward $K^+$ current reduction prolongs action potentials and promotes after-depolarizations: a dynamic-clamp study in human and rabbit cardiac atrial myocytes. J Physiol 590(17):4289–4305, PMID: 22733660, https://doi.org/10.1113/jphysiol.2012.235986.

72. Crotti L, Marcou CA, Tester DJ, Castelletti S, Giudicessi JR, Torchio M, et al. 2012. Spectrum and prevalence of mutations involving BrS1- through BrS12-susceptibility genes in a cohort of unrelated patients referred for Brugada syndrome genetic testing: implications for genetic testing. J Am Coll Cardiol 60(15):1410–1418, PMID: 22840528, https://doi.org/10.1016/j.jacc.2012.04.037.

73. Giudicessi JR, Ye D, Tester DJ, Crotti L, Mugione A, Nesterenko VV, et al. 2011. Transient outward current ($I_{to}$) gain-of-function mutations in the KCND3-encoded Kv4.3 potassium channel and Brugada syndrome. Heart Rhythm 8(7):1024–1032, PMID: 21349352, https://doi.org/10.1016/j.hrthm.2011.02.021.

74. Huang Y, Yang J, Xie W, Li Q, Zeng Z, Sui H, et al. 2017. A novel *KCND3* mutation associated with early-onset lone atrial fibrillation. Oncotarget 8(70):115503–115512, PMID: 29383177, https://doi.org/10.18632/oncotarget.23303.

75. Olesen MS, Refsgaard L, Holst AG, Larsen AP, Grubb S, Haunsø S, et al. 2013. A novel *KCND3* gain-of-function mutation associated with early-onset of persistent lone atrial fibrillation. Cardiovasc Res 98(3):488–495, PMID: 23400760, https://doi.org/10.1093/cvr/cvt028.

76. Takayama K, Ohno S, Ding WG, Ashihara T, Fukumoto D, Wada Y, et al. 2019. A *de novo* gain-of-function *KCND3* mutation in early repolarization syndrome. Heart Rhythm 16(11):1698–1706, PMID: 31173922, https://doi.org/10.1016/j.hrthm.2019.05.033.

77. Giudicessi JR, Ye D, Kritzberger CJ, Nesterenko VV, Tester DJ, Antzelevitch C, et al. 2012. Novel mutations in the *KCND3*-encoded Kv4.3 K+ channel associated with autopsy-negative sudden unexplained death. Hum Mutat 33(6):989–997, PMID: 22457051, https://doi.org/10.1002/humu.22058.

78. Kaese S, Verheule S. 2012. Cardiac electrophysiology in mice: a matter of size. Front Physiol 3:345, PMID: 22973235, https://doi.org/10.3389/fphys.2012.00345.

79. Knollmann BC, Katchman AN, Franz MR. 2001. Monophasic action potential recordings from intact mouse heart: validation, regional heterogeneity, and relation to refractoriness. J Cardiovasc Electrophysiol 12(11):1286–1294, PMID: 11761418, https://doi.org/10.1046/j.1540-8167.2001.01286.x.

80. Nowak MB, Veeraraghavan R, Poelzing S, Weinberg SH. 2021. Cellular size, gap junctions, and sodium channel properties govern developmental changes in cardiac conduction. Front Physiol 12:731025, PMID: 34759834, https://doi.org/10.3389/fphys.2021.731025.

81. King DR, Entz M II, Blair GA, Crandell I, Hanlon AL, Lin J, et al. 2021. The conduction velocity-potassium relationship in the heart is modulated by sodium and calcium. Pflugers Arch 473(3):557–571, PMID: 33660028, https://doi.org/10.1007/s00424-021-02537-y.

82. Quan W, Rudy Y. 1990. Unidirectional block and reentry of cardiac excitation: a model study. Circ Res 66(2):367–382, PMID: 2297808, https://doi.org/10.1161/01.res.66.2.367.

83. Shaw RM, Rudy Y. 1997. Ionic mechanisms of propagation in cardiac tissue. Roles of the sodium and L-type calcium currents during reduced excitability and decreased gap junction coupling. Circ Res 81(5):727–741, PMID: 9351447, https://doi.org/10.1161/01.res.81.5.727.

84. Rohr S, Kucera JP, Kléber AG. 1998. Slow conduction in cardiac tissue, I: effects of a reduction of excitability versus a reduction of electrical coupling on microconduction. Circ Res 83(8):781–794, PMID: 9776725, https://doi.org/10.1161/01.res.83.8.781.

85. Dominguez G, Fozzard HA. 1970. Influence of extracellular $K^+$ concentration on cable properties and excitability of sheep cardiac Purkinje fibers. Circ Res 26(5):565–574, PMID: 5443134, https://doi.org/10.1161/01.res.26.5.565.

86. King JH, Huang CLH, Fraser JA. 2013. Determinants of myocardial conduction velocity: implications for arrhythmogenesis. Front Physiol 4:154, PMID: 23825462, https://doi.org/10.3389/fphys.2013.00154.

87. Carll AP, Crespo SM, Filho MS, Zati DH, Coull BA, Diaz EA, et al. 2017. Inhaled ambient-level traffic-derived particulates decrease cardiac vagal influence and baroreflexes and increase arrhythmia in a rat model of metabolic syndrome. Part Fibre Toxicol 14(1):16, PMID: 28545487, https://doi.org/10.1186/s12989-017-0196-2.

88. Park H, Lim S, Lee S, Mun D, Kang J, Kim H, et al. 2021. High level of real urban air pollution promotes cardiac arrhythmia in healthy mice. Korean Circ J 51(2):157–170, PMID: 33525071, https://doi.org/10.4070/kcj.2020.0255.

89. Hou JW, Fei YD, Li W, Chen YH, Wang Q, Xiao Y, et al. 2018. The transient receptor potential melastatin 4 channel inhibitor 9-phenanthrol modulates cardiac sodium channel. Br J Pharmacol 175(23):4325–4337, PMID: 30153324, https://doi.org/10.1111/bph.14490.

90. Foth C, Gangwani MK, Ahmed I, Alvey H. 2023. Ventricular Tachycardia. In: *StatPearls*. Treasure Island, FL: StatPearls Publishing, PMID: 30422549.

91. Pogwizd SM. 1994. Focal mechanisms underlying ventricular tachycardia during prolonged ischemic cardiomyopathy. Circulation 90(3):1441–1458, PMID: 7522134, https://doi.org/10.1161/01.cir.90.3.1441.

92. Cherry EM, Fenton FH, Gilmour RF Jr. 2012. Mechanisms of ventricular arrhythmias: a dynamical systems-based perspective. Am J Physiol Heart Circ Physiol 302(12):H2451–H2463, PMID: 22467299, https://doi.org/10.1152/ajpheart.00770.2011.

93. Boukens BJ, Hoogendijk MG, Verkerk AO, Linnenbank A, van Dam P, Remme CA, et al. 2013. Early repolarization in mice causes overestimation of ventricular activation time by the QRS duration. Cardiovasc Res 97(1):182–191, PMID: 22997159, https://doi.org/10.1093/cvr/cvs299.

94. Akar FG, Rosenbaum DS. 2003. Transmural electrophysiological heterogeneities underlying arrhythmogenesis in heart failure. Circ Res 93(7):638–645, PMID: 12933704, https://doi.org/10.1161/01.RES.0000092248.59479.AE.

95. Akar FG, Spragg DD, Tunin RS, Kass DA, Tomaselli GF. 2004. Mechanisms underlying conduction slowing and arrhythmogenesis in nonischemic dilated cardiomyopathy. Circ Res 95(7):717–725, PMID: 15345654, https://doi.org/10.1161/01.RES.0000144125.61927.1c.

96. Mangat I, Dorian P. 2006. Chapter 31. Arrhythmias in the critical care setting. In: *Clinical Critical Care Medicine*. Albert RK, Slutsky A, Torres A, Takala J, eds. Maryland Heights, MO: Mosby, 319–341.

97. Vattanasit U, Navasumrit P, Khadka MB, Kanitwithayanun J, Promvijit J, Autrup H, et al. 2014. Oxidative DNA damage and inflammatory responses in cultured human cells and in humans exposed to traffic-related particles. Int J Hyg Environ Health 217(1):23–33, PMID: 23567252, https://doi.org/10.1016/j.ijheh.2013.03.002.

98. Jeng HA, Pan CH, Diawara N, Chang-Chien GP, Lin WY, Huang CT, et al. 2011. Polycyclic aromatic hydrocarbon-induced oxidative stress and lipid peroxidation in relation to immunological alteration. Occup Environ Med 68(9):653–658, PMID: 21126960, https://doi.org/10.1136/oem.2010.055020.

99. Yan Y, Wei C, Zhang WR, Cheng HP, Liu J. 2006. Cross-talk between calcium and reactive oxygen species signaling. Acta Pharmacol Sin 27(7):821–826, PMID: 16787564, https://doi.org/10.1111/j.1745-7254.2006.00390.x.

100. Rossi S, Fortunati I, Carnevali L, Baruffi S, Mastorci F, Trombini M, et al. 2014. The effect of aging on the specialized conducting system: a telemetry ECG study in rats over a 6 month period. PLoS One 9(11):e112697, PMID: 25398004, https://doi.org/10.1371/journal.pone.0112697.

101. Savi M, Rossi S, Bocchi L, Gennaccaro L, Cacciani F, Perotti A, et al. 2014. Titanium dioxide nanoparticles promote arrhythmias via a direct interaction with rat cardiac tissue. Part Fibre Toxicol 11(1):63, PMID: 25487314, https://doi.org/10.1186/s12989-014-0063-3.

102. Lacampagne A, Duittoz A, Bolaños P, Peineau N, Argibay JA. 1995. Effect of sulfhydryl oxidation on ionic and gating currents associated with L-type calcium channels in isolated guinea-pig ventricular myocytes. Cardiovascular Research 30(5):799–806, PMID: 8595629, https://doi.org/10.1016/S0008-6363(95)00128-X.

103. Gill JS, McKenna WJ, Camm AJ. 1995. Free radicals irreversibly decrease $Ca^{2+}$ currents in isolated guinea-pig ventricular myocytes. Eur J Pharmacol 292(3–4):337–340, PMID: 7796875, https://doi.org/10.1016/0926-6917(95)90042-x.

104. University of Nottingham. 2023. ActionPotential-Portal application. https://cardiac.nottingham.ac.uk/ActionPotentialPortal/ [accessed 5 May 2023].